A BASE AND PRECIOUS METAL STUDY OF BIF ASSOCIATED INTERFLOW METASEDIMENTS, KIRKLAND LAKE, ONTARIO.

A BASE AND PRECIOUS METAL STUDY OF BIF ASSOCIATED INTERFLOW METASEDIMENTS, KIRKLAND LAKE, ONTARIO.

By

Albert G. Chong

Submitted to the Department of Geology
in Partial Fulfillment of the Requirements for
the Degree Bachelor of Science

McMaster University

April, 1985.

BACHELOR OF SCIENCE (1985) McMASTER UNIVERSITY
(Geology) Hamilton, Ontario.

TITLE: A Base and Precious Metal Study of BIF Associated Interflow Metasediments, Kirkland Lake, Ontario.

AUTHOR: Albert G. Chong

SUPERVISOR: Dr. J.H. Crocket

NUMBER OF PAGES: ix, 75

ABSTRACT

The interflow sediments studied are part of the Boston iron range in the Larder Lake Group near Kirkland Lake, Ontario. Due to the proximity of the Lebel stock, transitional contact metamorphism between hornblende-hornfels facies and albite-epidote-hornfels facies has been inferred for the study area. A later regional overprint of lower greenschist facies has also been interpreted.

Base metal mineralization in the area is Zn rich. However, it is not genetically related to the BIF. Instead, the base metal mineralization may have been introduced during the intrusion of the Lebel stock by metasomatic processes associated with contact metamorphism.

Anomalous Au abundances (> 10 ppb) in the study area is inferred to be associated with sulphide mineralization and possibly active carbon. Sulphide samples associated with anomalous Au concentrations usually display the annealing recrystallization of fine grained cataclastic pyrite. A statistically positive correlation between Zn and Au was also determined. This may imply that the Au was introduced synchronously with or post intrusion of the Lebel stock. Anomalous Au values in

the chemical sediments were noted to coincide with high As and Sb concentrations.

ACKNOWLEDGEMENTS

The production of this thesis was accomplished with the help of many special individuals. Therefore, I would like to express my gratitude to the following persons. First, I would like to thank the technicians Abdul Kabir, Oto Mudroch, Len Zwicker, Jack Whorwood and Tom Bryner for their expertize and time. Also, thanks must be extended to Steve Bonnyman, Mark Hughes, and J.H.C's stable of brains (Gordon McRoberts, Andy Fyon, Norbert Blum, Bob Bowins, Tracey Hurley, Jonathan Inman and Robert Moritz) for lending their time and advice.

Special thanks is reserved for Dr. J.H. Crocket for supervising this thesis and having confidence in me.

Lastly, I would like to thank 5:30 p.m. M*A*S*H for sharing my suppers and Chester Carlson for inventing the photocopy machine.

Funding was provided in part by the Ontario Geoscience Research Grant Program.

TABLE OF CONTENTS

LIST OF FIGURES

LIST OF PLATES

LIST OF TABLES

CHAPTER 1

INTRODUCTION:

1.0 LOCATION:

The samples used as the basis for this thesis are from an 11.5 sq. km area immediately west of the Adams mine. The Adams mine is located approximately 12 km southeast of Kirkland Lake, Ontario in Boston Township (see Figure 1.1), approximately 11 km east of Highway 11 via the Adams Mine Road.

1.1 PREVIOUS GEOLOGICAL WORK:

Systematic geological work in the Adams mine area was initiated by the Dominion Gulf Company in 1948. This included an airborne magnetometer survey, reconnaissance mapping, ground magnetometer surveys, sampling, and drilling. The property was optioned to Jones and Laughlin in 1954 who later developed the Adams open pit mine producing 1,000,000 tons of iron ore pellets annually. The property was sold to Dominion Foundaries and Steel, Limited of Hamilton (Dofasco) in 1971 with Cliffs of Canada acting as managers (Dubuc, 1972; Jensen, 1978a). Dubuc (1972) later produced a report on the geology of the Boston iron range delineating the economic banded iron

FIGURE 1.1: LOCATION AND GENERAL GEOLOGY MAP OF THE KIRKLAND LAKE - LARDER LAKE AREA

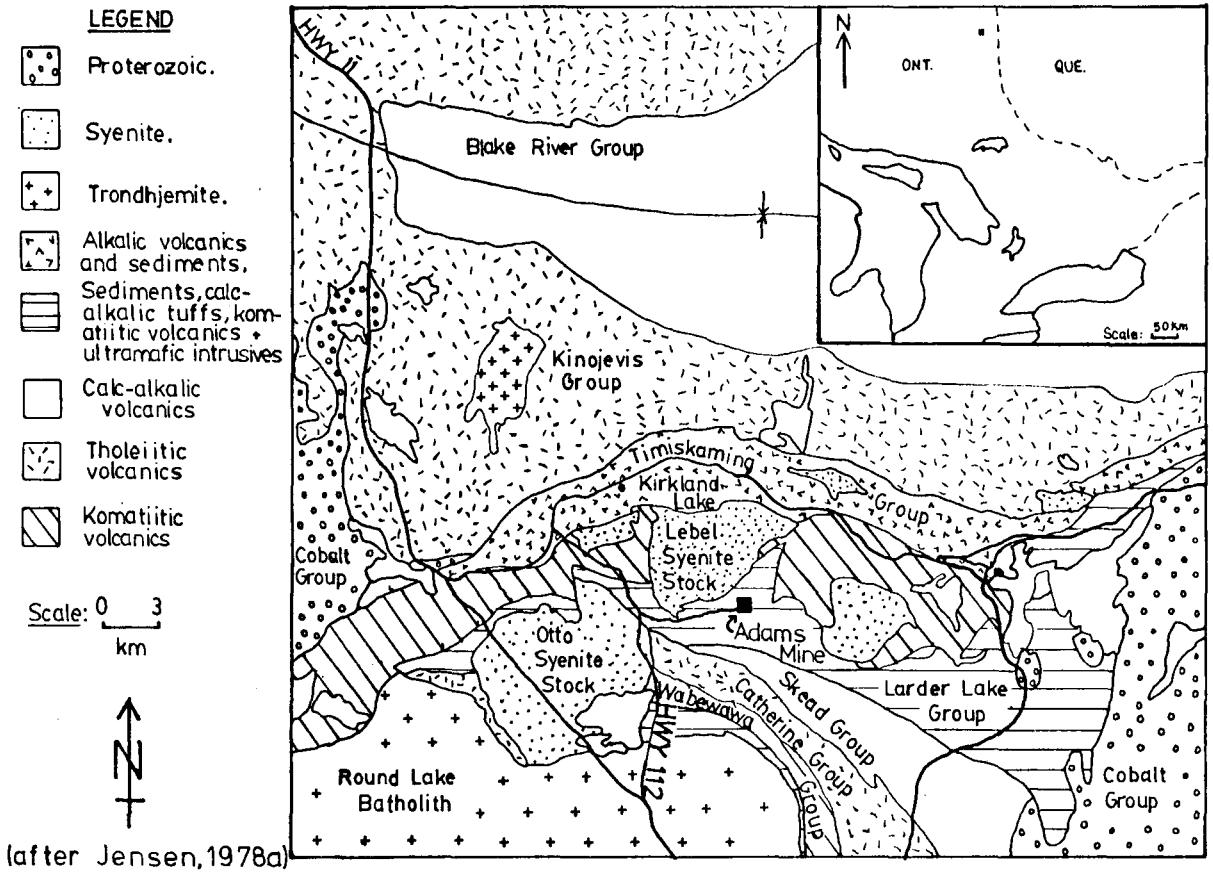

formation (BIF) and some of the surrounding country rock in a 1:36,000 scaled map. In 1983, a MSc. thesis involving the detailed study of stratigraphy, petrography and geochemistry of an area immediately west of the South pit was initiated by Gordon McRoberts of McMaster University. The study included ground both within and beyond the bounds of the mine property.

1.2 OBJECTIVE OF THESIS:

This thesis is part of a much larger study whose major objective is to evaluate possible genetic relationships between BIF and other mineralization (Crocket et al., 1983). With this objective in mind, an investigation of the genesis of BIFs and their relationships with the surrounding volcanosedimentary host rocks was undertaken. Ultimately, this study may evaluate the usefulness of Archean BIF as an exploration guide to precious and base metal mineralization and deposition.

The objective of this thesis is to classify and determine possible relationships of precious and base metal mineralization within a suite of interflow sedimentary rocks. These sediments are thought to be closely related stratigraphically to the South pit economic BIF of the Adams mine (McRoberts, 1985), and are a part of Gordon McRoberts' MSc. field study area.

1.3 METHODOLOGY:

The samples for this study were collected by Gordon McRoberts in a detailed sampling and mapping program of an area west of the Adams mine South pit during the 1983-84 field seasons. The area is bordered by the Lebel syenite stock to the north and the Boston fault (as named by Lawton, 1957) to the southeast. The physiographic and geological location of the samples are shown in MAP 1 (in sleeve at the back). The samples chosen for analysis were mapped as detrital sediments, siliceous chemical sediments (cherts), graphitic chemical sediments (graphitic cherts) and sulphide-rich rocks. The samples under study are not all from the same unit and have varying statigraphic relationships with respect to the BIF.

Nineteen polished thin and thin sections were studied under reflecting and transmitted optical microscopy. Major and trace element analyses for 25 samples were obtained by X-Ray Fluorescence (XRF) and Au, As, W and Sb were determined by Epithermal Instrumental Neutron Activation Analysis (EINAA). An acid evolution-gravimetric method and LECO determination was used to analyze the carbonate carbon content, while loss on ignition (LOI) was used to determine the volatile content. These data helped to classify the rocks and determine any

systematic relationships between the major and trace elements and precious and base metals.

CHAPTER 2

GENERAL GEOLOGY:

2.0 REGIONAL STRATIGRAPHY OF THE KIRKLAND LAKE - LARDER LAKE AREA:

The area under study is southeast of Kirkland Lake and part of the Abitibi greenstone belt of the Superior province (see Figure 1.1). Two major volcanic cycles and a possible older, relict volcanic cycle have been identified in the Kirkland Lake area by Jensen (1978a). In this paper, Jensen defines a volcanic cycle as having a basal komatiitic sequence, a middle tholeiitic sequence and an upper calc-alkaline sequence. The volcanic cycles are separated by a sedimentary zone containing conglomerate, argillite, chert and BIF.

Jensen (1978a, 1978b, 1979) has also described the region as a large synclinorium approximately 80 to 120 km wide that plunges to the east. The youngest volcanic cycle is in the north limb while the two older cycles make up the south limb of the synclinorium. Jensen (1976) also mentions that the oldest volcanic cycle in the south limb may be a relict volcanic cycle which was truncated by the Round Lake Batholith further to the south. The stratigraphy of the Kirkland Lake - Larder Lake area may be

seen in Figure 1.1.

Prior to 1978, sediments in the area were defined as part of the Timiskaming Group by workers such as Lawton (1957), Hewitt(1963) and Ridler (1970). However, the eastward extension of Lawton's Timiskaming Group showed that some of the sedimentary rocks were interlayered with calc-alkalic and komatiitic volcanic rocks. This suggested that the sediments were older and equivalent in age to the Boston iron range (Jensen, 1977). These interlayered sediments and volcanic flows were reclassified as the Larder Lake Group by Jensen (1978b).

2.1 GEOLOGY OF THE BOSTON IRON RANGE:

2.1.1 GENERAL STRATIGRAPHY:

The Boston iron range is found within the Larder Lake Group. The Larder Lake Group is the basal komatiitic section of the youngest volcanic cycle in the south limb of Jensen's synclinorium and unconformably overlies the Skead Group which is at the top of the older relict volcanic cycle further to the south (Jensen, 1978b). It consists of peridotitic komatiites, basaltic komatiites and Mg-rich tholeiitic basalts interlayered with turbiditic conglomerate, greywacke, argillite, carbonate and BIF (Jensen, 1978b).

Eight volcanic sequences have been described and

mapped to the west of the BIF by McRoberts (1985). The oldest volcanic sequence, which overlies the Skead pyroclastics, consists of tholeiitic and calc-alkalic basalt. The remaining sequences are generally characterized by basal ultramafic komatiite , followed by high and low MgO komatiitic basalts, with a low MgO komatiitic andesite or a high Al203- low Mg- komatiitic basalt at the top of the sequence. The terminology used above to describe the volcanics is from McRoberts (1985). It differs from conventional terminology previously used to describe basic volcanic rocks because of their unusual geochemical nature.

McRoberts (1985) noted the presence of twelve interflow metasedimentary horizons. These metasedimentary horizons are stratigraphically above, below and equivalent to the economic BIF and are clastic and chemical in origin. It is from these metasedimentary horizons that the samples for this study have been chosen.

2.1.2 IRON FORMATION:

The Boston iron range is an Archean Algoman type iron formation (Gross, 1965). Crocket et al. (1984) have proposed that there are three major economic BIF bands. Cycle I (the oldest cycle) includes the Peria and South pits, cycle II (the intermediate cycle) the Central and

North Central pits, and cycle III (the youngest cycle) consists of the West and West Central pits. To the west of the mine site there are at least two bands of uneconomic BIF. They are believed to be stratigraphically equivalent to the South pit BIF (Crocket et al., 1984; McRoberts, 1985; Blum, 1985).

2.1.3 INTRUSIVES:

The Boston iron range and its surrounding volcanosedimentary pile have been intruded and deformed by the Lebel syenite stock. The stock covers the southern half of Lebel township to the north and stretches about 2.5 km into the north part of Boston Township. As noted previously in the methodology section, the Lebel syenite stock represents the northernmost boundary of McRoberts' field area. Samples were taken up to 575 m from the stock. Therefore, one can not ignore the possible effects of contact metamorphism.

Sills in the area are peridotitic, pyroxenitic, gabbroic, and microgabbroic in composition (McRoberts, 1985). The sills are believed to represent the intrusive equivalent of the tholeiitic flows of the surrounding country rock (Jensen, 1976).

Three distinct types of dykes found in the area are syenite, lamprophyre and diabase as described by Dubuc

(1972). The syenite dykes have a general N-S and NW-SE orientation while the lamprophyre dykes trend NE-SW and E-W. The diabase dykes are the youngest of all the dykes and are generally uncommon (Dubuc, 1972).

2.1.4 STRUCTURE:

The Boston iron range mimics the southern outline of the Lebel stock in an arcuate curve and is cross-cut by fracture and fault zones radiating out perpendicular from the stock (Dubuc, 1972). Lawton (1957) first noted the presence of a major syncline with an axial strike of N35°E. Dubuc (1972) confirmed the existence of the syncline and noted that it had a southwesterly plunge of about 50°-60°. This syncline is also noted further to the southwest by McRoberts (1985) even though a plunge was not determined. McRoberts (1985) referred to this syncline as the Lebel syncline, and this term is adapted here. The strata hosting the BIF are part of the south limb of the Lebel syncline and have dips of approximately 80° NW and a strike between N30°E to N45°E.

CHAPTER 3

PETROGRAPHY:

3.0 SAMPLE CLASSIFICATION:

The samples have been put into one of three classes. These classes are the carbonaceous chemical sediments (CCS), the non-carbonaceous chemical sediments (NCS) and the clastic sediments (CS). The CCS all contain a black, fine-grained, isotropic mineral which is usually smeared out due to polishing of the thin section. In the field, these rocks were termed graphitic cherts. Graphite has been defined by some authors as a mineral consisting of graphitic carbon regardless of its crystalline perfection (Wilson, 1985). An additional criterion proposed by Wilson (1985) is that the graphite must have a 3-dimensional structure. This definition distinguishes true "graphite" from amorphous carbon. The samples were not analyzed for crystal structure by diffraction methods; therefore, any samples which contained any possible graphite were classified as a carbonaceous chemical sediment. Only the presence of carbon in the thin sections was required for the sample to be placed in this class.

The chemical sediments are characterized by having a fine-grained siliceous appearance in hand sample and the

presence of microcrystalline and/or recrystallized quartz in thin section. They are thought to be the product of chemical precipitation. The abundance of fine grained and recrystallized coarser grained quartz is between 20 to 70 modal percent. The recrystallized quartz has unstrained extinction, polygonal form and is about 1.5 mm in size.

The clastic sediments generally have lower quartz and higher plagioclase feldspar modal abundances than the chemical sediments. They are believed to be clastic in origin due to the presence of coarse grained quartz and feldspar clasts enclosed in a fine grained silicious matrix. These sediments are part of turbiditic sequences in the area. The chemical sediments are probably part of the E Bouma series units and the clastic sediments part of the A Bouma units.

3.1 METAMORPHISM:

3.1.1 METAMORPHIC GRADE:

Rocks in two metamorphic grades have been identified for the area; one of regional and the other of contact origin. Some rocks exhibit a metamorphic grade which appears to be transitional between upper epidote-amphibolite facies and lower amphibolite facies. The minerals present which indicate a low amphibolite grade facies are plagioclase feldspar (An>25), hornblende,

garnet, diopside (see Plates 3.1 and 3.2) and cordierite. However, both albite (An>5) and oligoclase (An>20) exist in the same thin section. The presence of albite implies that there has not been a full development of the amphibolite facies (Turner, 1981). Further evidence that the grade bridges the greenschist-amphibolite facies transition, besides the presence of hornblende (see Plate 3.3) and garnet (see Plates 3.4 and 3.5), is the continuing presence of chlorite and epidote.

The ACF diagram for the regional metamorphism may be found in Figure 3.1. Stilpnomelane occurs as brownish-red felted masses in individual rectangular blades of approximately 0.1 mm in length. It has been observed in the matrix of samples in all three classes, hydrothermal quartz veins, and intergrown with pyrite (see Plate 3.6). The intergrowth of the pyrite and stilpnomelane implies that the minerals were formed synchronously. As indicated by Table 3.1, stilpnomelane is found to occur predominantly in the non-carbonaceous samplies regardless of distance to the Lebel stock. Also, according to Turner (1981), stilpnomelane is never formed by contact metamorphism. Therefore, the stilpnomelane and the associated pyrite was formed after the intrusion of the Lebel stock by a regional metamorphic overprint represented by a lower greenschist facies (chlorite zone) assemblage.

TABLE 1: POLISHED THIN AND THIN SECTION TRANSMITTED LIGHT MINERALOGY

		MINERALOGY (MODAL %)																
	SAMPLE	C. CARBON	QUARTZ MATRIX	QUARTZ VEIN	?	GAR.	CORD.	HBL.	DIOP.	EPID. GROUP	CHL. GROUP	STILP.	TREM.-ACTIN.	PLAG.	MUSC.	SER.	CT.	ZIR.
A	M-320	35	40	5	9	--	--	--	--	4	--	--	--	--	--	--	--	--
	M-279	35	25	10	7	--	--	--	--	4	--	--	9	--	--	--	--	--
	M-647	4	74	7	--	--	--	--	--	--	--	6	--	--	3	--	--	--
	M-065	65	25	--	--	--	--	--	3	2	--	--	--	--	3	--	2	--
	M-781	20	65	10	--	--	--	--	--	2	--	--	--	--	--	--	--	--
	M-755B	5	77	7	--	--	--	--	--	--	--	3	--	--	3	--	tr	tr
	M-146	15	40	12	--	--	--	--	--	--	--	--	--	5	--	23	--	--
	M-408	20	32	3	--	--	--	--	--	--	--	--	2	10	--	--	--	--
B	M-784	--	39	--	1	10	--	2	4	15	--	7	--	3	--	--	3	--
	M-419	--	20	--	--	3	--	--	--	11	--	3	42	--	1	--	--	--
	M-415	--	45	--	--	--	--	10	--	8	3	12	10	--	--	--	--	--
	M-774A	--	66	--	--	--	--	--	--	--	12	12	--	--	--	--	--	--
	M-774B	--	70	--	--	--	--	--	--	--	10	5	--	--	--	--	--	--
	M-775A	--	32	10	--	--	--	--	--	--	--	--	--	1	2	30	--	--
	M-771	--	78	2	--	--	--	--	--	--	--	8	--	--	--	12	--	--
	M-783	--	60	--	--	--	--	12	--	--	8	6	--	2	1	--	2(?)	tr
	M-089	--	68	5	--	--	--	--	--	8	--	3	4	5	--	--	2	--
C	M-211	--	30	--	--	--	2	5	--	2	3	tr	--	10	--	--	--	--
	M-592	--	10	--	--	--	2	--	--	7	--	13	--	17	--	5	--	tr

EXPLANATION

A - Carbonaceous Chemical Sediment; B - Non-Carbonaceous Chemical Sediment; C - Clastic sediment; tr - trace; -- indicates feature not present in sample. Mineral abbreviations as follows: C. - Carbonaceous; GAR. - Garnet; CORD.- Cordierite; HBL.- Hornblende; DIOP.- Diopside; EPID.- Epidote; CHL.- Chlorite; STILP.- Stilpnomelane; TREM.-ACTIN.- Tremolite-Actinolite; PLAG.- Plagioclase; MUSC.- Muscovite; SER.- Sericite; CT.- Calcite; ZIR.- Zircon

PLATE 3.1: Diopside (A) with diallage enclosed in pyrite and quartz exhibiting strained extinction. From M-784 under polarized transmitted light (63x).

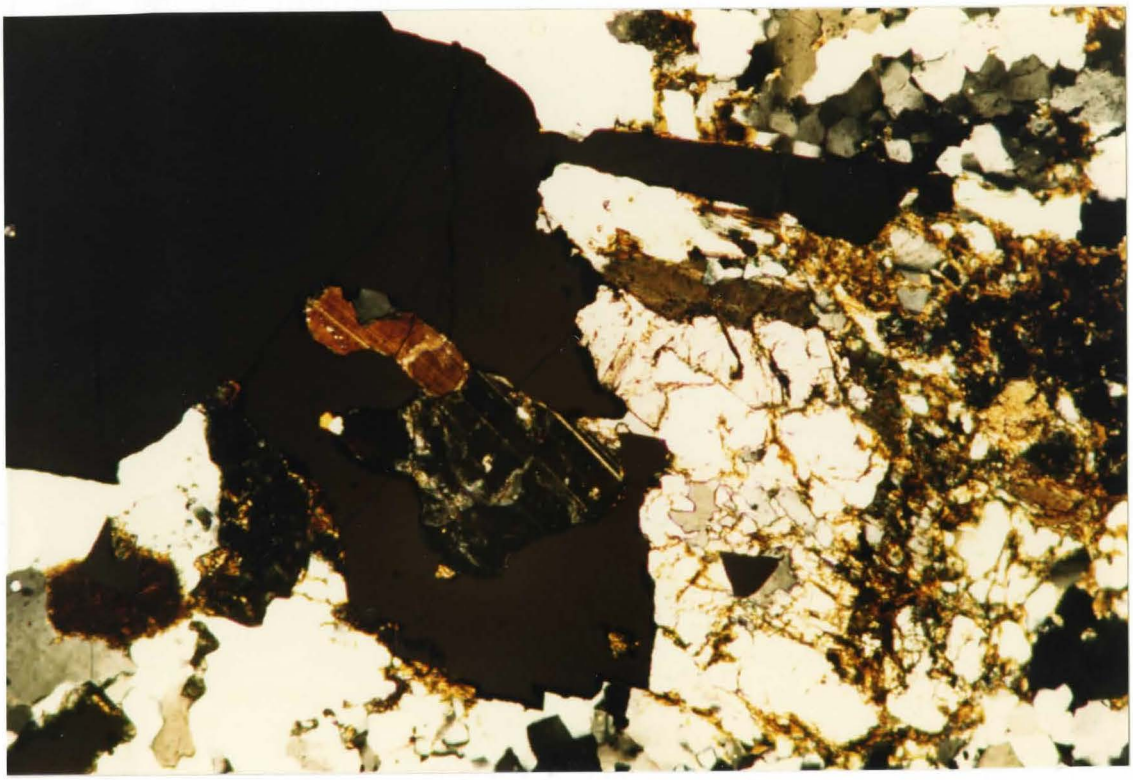

PLATE 3.2: Diopside exhibiting 45° extinction. Under polarized transmitted light (63x).

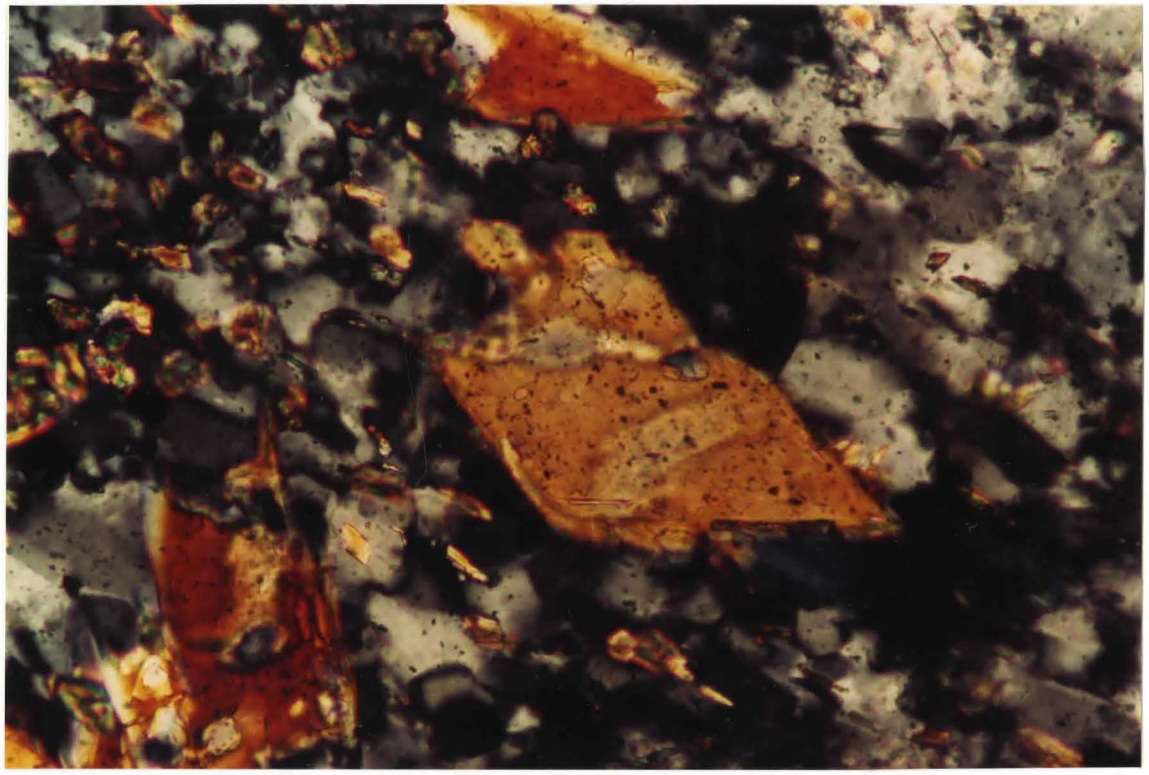

PLATE 3.3: Hornblende section parallel to (010). From M-783 under polarized transmitted light (250x).

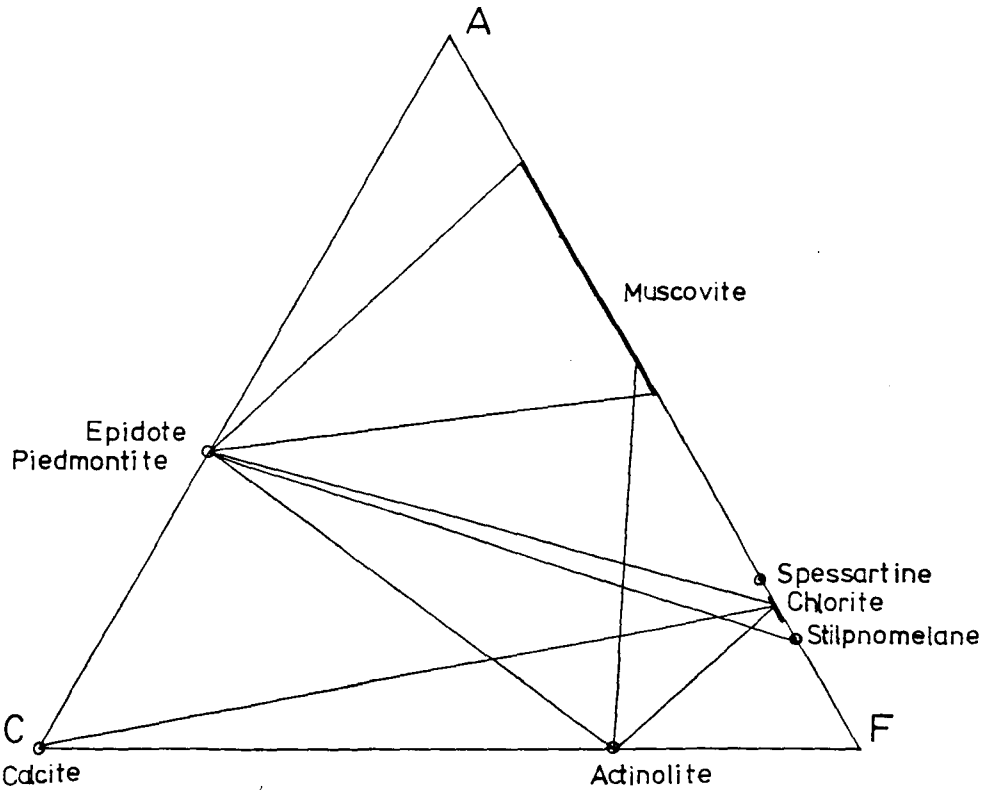

Figure 3.1: ACF diagram showing the lower greenschist (chlorite zone) equilibrium assemblage for the regional metamorphism.

3.1.2 CONTACT METAMORPHISM AND METASOMATISM:

The intrusion of the Lebel stock is responsible for contact metamorphism and probably metasomatism in the area. Evidence for contact metamorphism is implied by the mineralogy of the rocks in the vicinity of the Lebel stock. Generally, there is an increase in metamorphic grade as the distance to the Lebel stock decreases. The principle minerals which indicate metamorphic grade are garnet and diopside. Both the geographic position and the abundances of garnet and diopside in the samples are diagnostic of grade.

More than one type of garnet is present. Some exhibit weak anisotropism and zoning while others are isotropic (see Plate 3.4). The anisotropic zoned garnets probably belong to the ugrandite series while the isotropic garnets are part of the pyralspite series. The ugrandite garnets present are possibly andradite as suggested by the high CaO and low Al2O3 contents for M-784 and M-419 relative to Cameron and Garrels' (1980) values found in Table 4.1. In a study of the contact qureole surrounding the Otto stock, Jolly (1978) has noted the presence of andradite. Andradite typically occurs in contact or thermally metamorphosed impure calcareous sediments and in metasomatic skarn deposits where Fe2O3 and SiO2 have been added to the system (Deer, Howie, and Zussman, 1980).

The pyralspite series of garnets may be represented by spessartine and almandine. Spessartine is characterized by high MnO (as in M-784 and M-419) which may be due to metasomatism associated with adjacent igneous intrusions or with a more widespread regional metasomatism. It is also known from veins in greywackes and in significant amounts with almandine from igneous and metamorphic rocks associated with thermal aureoles (Deer, Howie and Zussman, 1980). Therefore, the presence of andradite and spessartine reinforces the possibility of contact metamorphism. If contact metamorphism is the case for the study area, the inferred metamorphic facies would be transitional between hornblende-hornfels facies and albite-epidote-hornfels facies. This metamorphic grade would then have been followed by regional metamorphism of lower greenschist facies.

Metasomatism of the area is represented by silicification, the sericitization of plagioclase feldspar (see Plate 3.7), and the introduction of various cations and anions (Moorehouse, 1959) such as S , Fe, Zn and Mn; probably represented in the minerals pyrite, sphalerite and garnet respectively. Metasomatic quartz is considered to be the same as hydrothermal quartz and is coarse grained (Moorehouse, 1959) with undulose extinction. The hydrothermal quartz veinlets found in the sections are 0.5

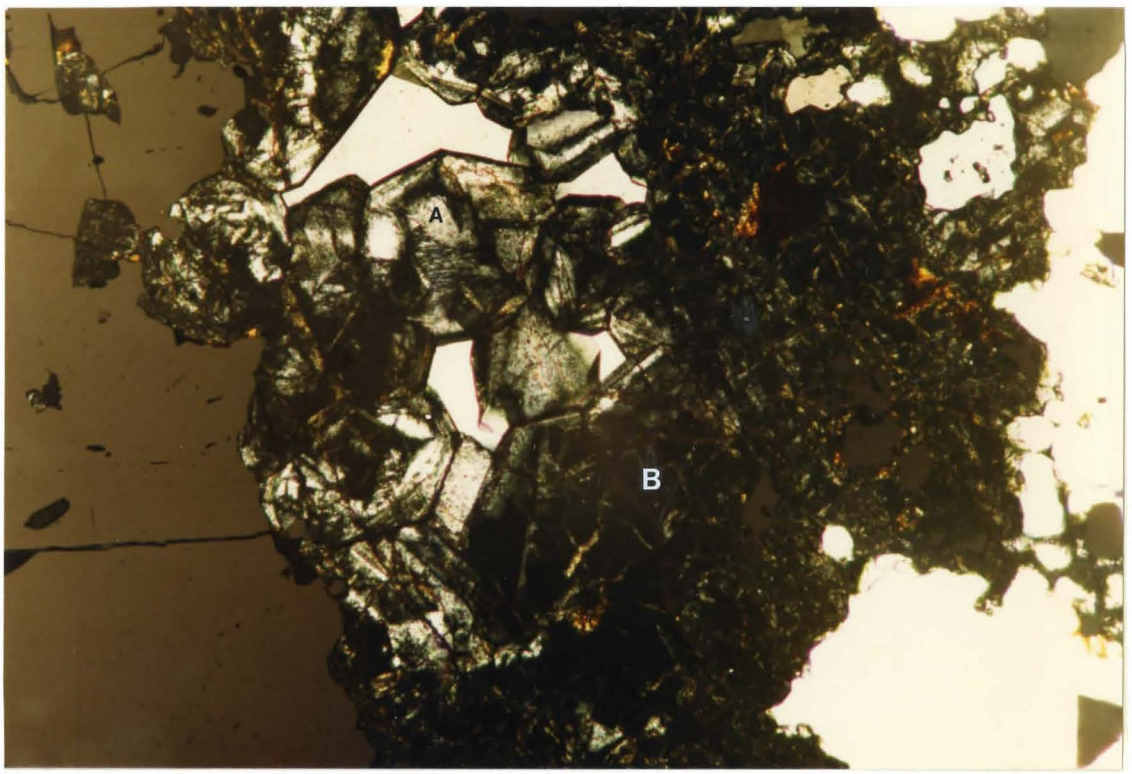

PLATE 3.4: Zoned garnet exhibiting anisotropism (A) and isotropism (B). From M-784 under polarized transmitted light (63x).

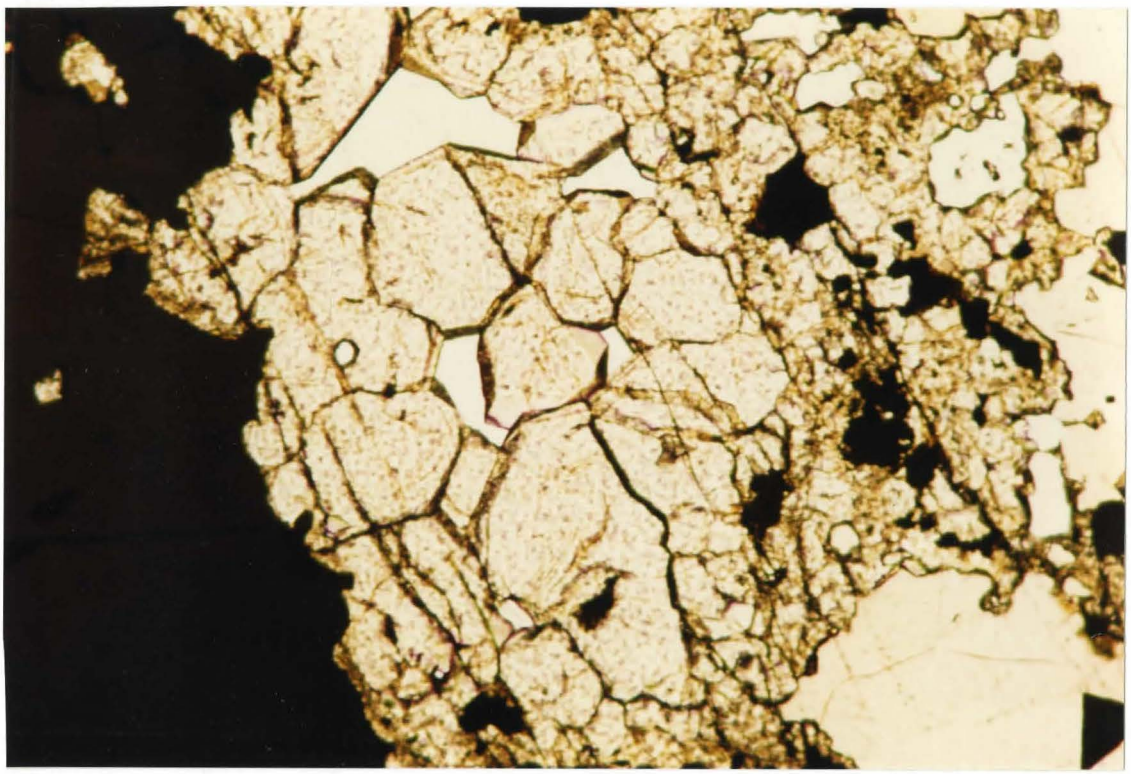

PLATE 3.5: Garnet showing euhedral and anhedral form.
From M-784 under transmitted plane light (63x).

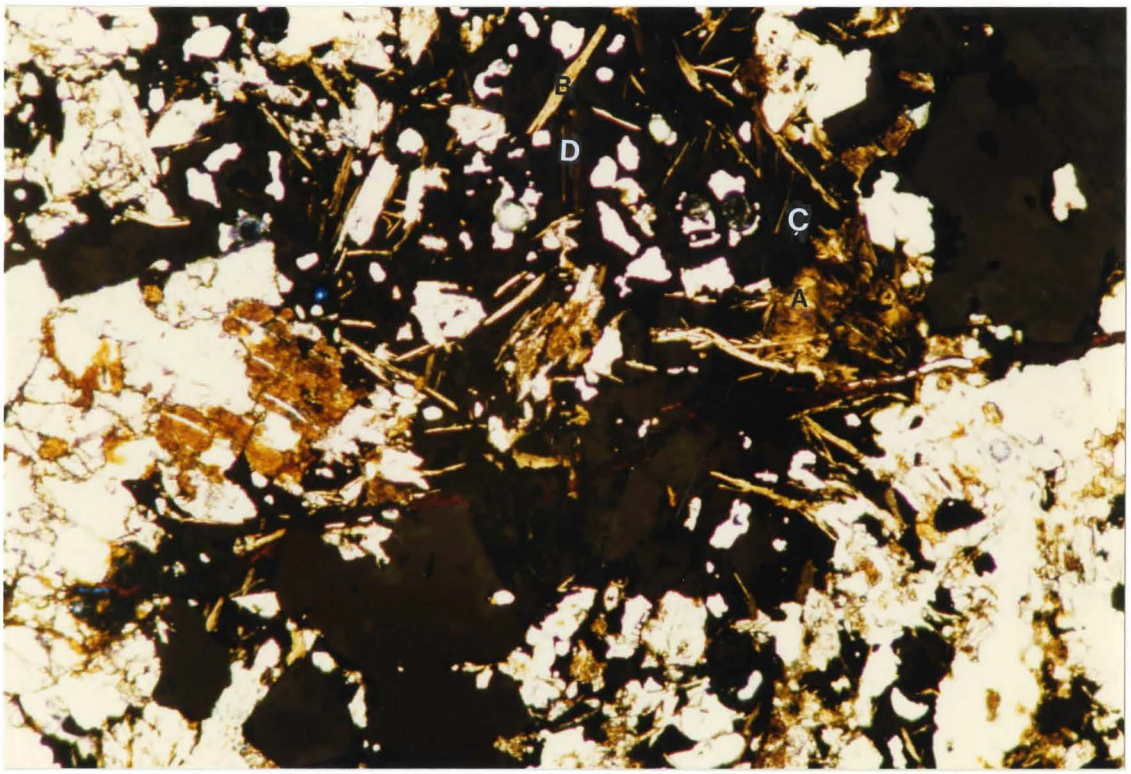

PLATE 3.6: Felted masses (A) and rectangular blades (B) of stilpnomelane intergrown with pyrite (C). Stilpnomelane also shows parallel to sub-parallel extinction (D). From M-419 under transmitted partially polarized light (63x).

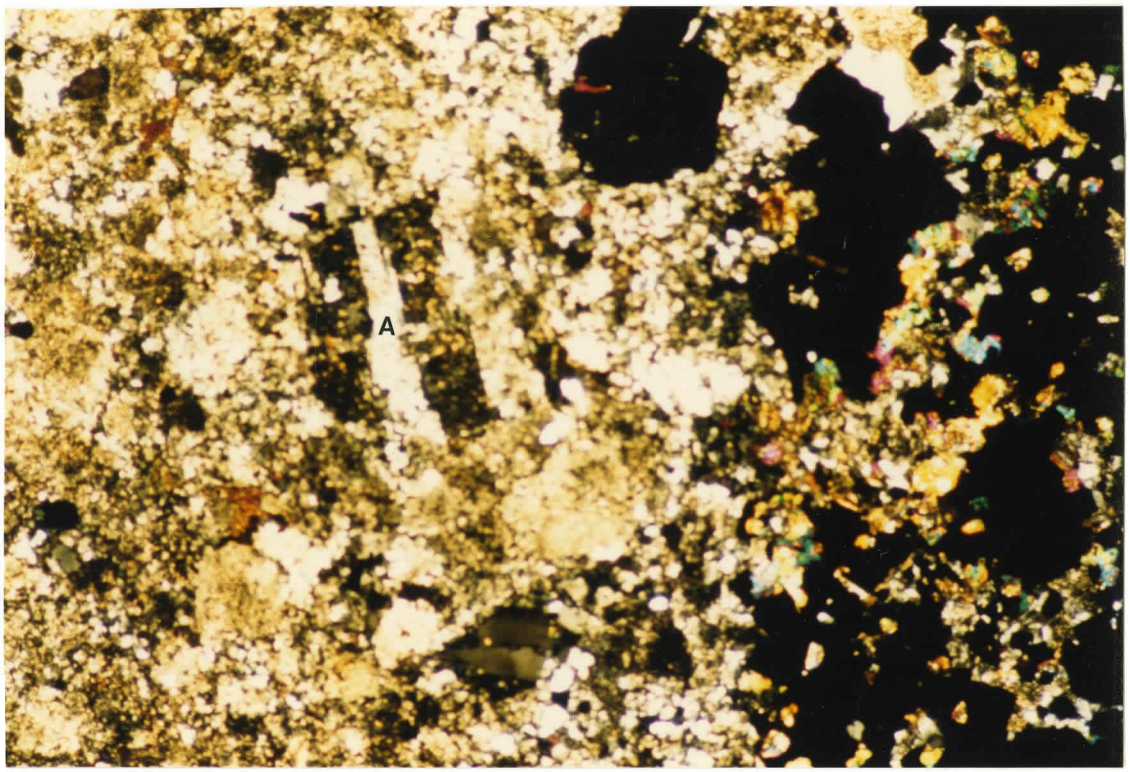

PLATE 3.7: Sericitized plagioclase (A) showing albite twinning. Also, note the highly birefringent epidote. From M-211 under transmitted polarized light (25x).

to 1.0 mm in width and typically make up only 2 to 10 percent of a slide. They are randomly oriented in the sections where present. The cross-cutting nature of these veinlets suggest that they either post-date or are synchronous with the metamorphism.

Mineral changes associated with the introduction of sulphur have brought the formation of hydrothermal sulphides such as pyrite, pyrrhotite, and sphalerite. Also, Jolly (1978) has attributed the formation of clinozoisite, hematite, and andradite, in a contact aureole surrounding the Otto stock, to a high fO2 resulting from the introduction of hydrothermal fluids during the intrusion of a volatile rich alkaline stock. Another source for solutions producing metasomatism is connate water trapped in the sediments and surrounding volcanics (Moorehouse, 1959).

3.1.3 DYNAMIC METAMORPHISM:

The metamorphic textures illustrating mechanical deformation of the area are the strain extinctions of quartz, schistosity due to the foliation of stilpnomelane, muscovite, and sericite and the single occurrence of an augen texture around a grain of polycrystalline quartz in M-146. Since stilpnomelane helps define the foliation, one may infer that part of the dynamic metamorphism is due to

regional deformation. Another source of deformation would be the intrusion of the Lebel stock. Dynamic metamorphic textures observed in the sulphides will be discussed in the reflected light petrography section.

3.2 REFLECTED LIGHT PETROGRAPHY:

The metallic minerals present in polished thin sections are pyrite, pyrrhotite, pentlandite, sphalerite, chalcopyrite, magnetite and chromite. The estimated modal percentages of the various minerals may be found in Table 3.2. In general, the sulphide minerals occur as disseminated grains throughout a section, as fracture controlled grains and in concentrated recrystallized zones.

Due to structural deformation and the proximity of the study area to the Lebel stock, textures are expected to reflect both regional and contact metamorphism. Cataclastic deformation and recrystallization can be expected to result from deformation whereas contact metamorphism should promote recrystallization and remobilization of existing sulphides and the development of new sulphide phases (Spry, 1976; Stanton, 1972).

The textural evidence for metamorphism includes cataclastic pyrite (see Plate 3.8), annealing recrystallization of fine grained cataclastic pyrite (see Plate 3.9), epitaxial growth of secondary pyrite on primary

pyrite (see Plates 3.10 and 3.11), atoll structures in pyrite, subgraining of pyrrhotite and very minor remobilization of chalcopyrite. All samples with > 5 modal percent sulphide, regardless of petrographic class (ie. CCS, NCS and CS), exhibit deformation textures. Mechanical deformation may be directly linked to the intrusion of the Lebel stock since the local stratigraphy of the Boston iron range is an arcuate curve which mimics the outline of the stock.

The polymetamorphism of the pyrite indicates a complex history of deformation in the area. The intergrowth of subhedral and euhedral pyrite with metamorphic silicate minerals, such as stilpnomelane (see Plate 3.6), shows that some of the pyrite was formed synchronously with the metamorphic silicates (Py III). The anhedral pyrite with silicate + chalcopyrite + pyrrhotite inclusions and atoll textures are indicative of a selective secondary replacement process (Spry, 1976) where silicate is replacing pyrite (Py I). The minor chalcopyrite inclusions are problably due to the growth of pyrite around such inclusions whereas the pyrrhotite inclusions may be an alteration product due to sulfur loss (Crocket, personal communication). The cataclastic pyrite found in slides M-415 and M-755B best exemplify the polymetamorphism of the sulphide minerals in the area as they reflect both

TABLE 2: POLISHED THIN SECTION REFLECTED LIGHT MINERALOGY AND TEXTURES

		Mineralogy (Modal %)							Textures						
	Samples	Py	Po	Pn	Sph	Cpy	Mt	Cr	Cataclastic Defm.	Recrystal-lization	Over growths	Po Sub-grains	Atoll structures	Remobil-ization	Corona-Colloform
A	M-320*	tr	1.5	1.5	2	1	--	--	--	--	--	--	--	--	+
	M-279	3.5	3.5	tr	3	tr	--	--	--	--	--	--	--	--	+
	M-065	--	--	--	--	--	--	--	--	--	--	--	--	--	--
	M-781	2	--	--	1	--	--	--	--	--	--	--	--	--	--
	M-755B*	10	--	--	tr	--	--	--	+	+	--	--	--	--	--
	M-408	2	4	--	1	1	--	--	--	--	+	+	--	--	+
B	M-784	14	2	tr	--	--	2	--	--	--	+	--	+	--	+
	M-419	3	5	5	2	1	--	--	--	--	--	--	--	--	--
	M-415	8	--	--	--	--	--	4	+	--	--	--	--	--	--
	M-774 A	10	--	--	--	tr	--	--	--	--	+	--	+	--	--
	B	13	--	--	2	--	--	--	--	--	+	--	+	--	--
	M-775A*	20	2	--	--	--	--	--	+	+	--	--	--	--	--
	M-783	4	3	tr	--	tr	--	--	--	--	--	--	--	--	+
	M-89	--	--	--	--	--	--	--	--	--	--	--	--	--	--
C	M-211*	10	tr	--	2	--	--	--	+	+	--	--	+	--	--
	M-592	40	1	--	--	2	3	--	+	--	--	--	+	--	--

EXPLANATION

* Au values >10 ppb; A - Carbonaceous Chemical Sediment; B - Non-Carbonaceous Chemical Sediment; C - Clastic sediment; tr - trace; + indicates feature present in sample; — indicates feature not present in sample.

Mineral abbreviations as follows: Py - pyrite; Po - pyrrhotite; Sph - sphalerite; Cpy - chalcopyrite; Mt - magnetite; Cr - chromite

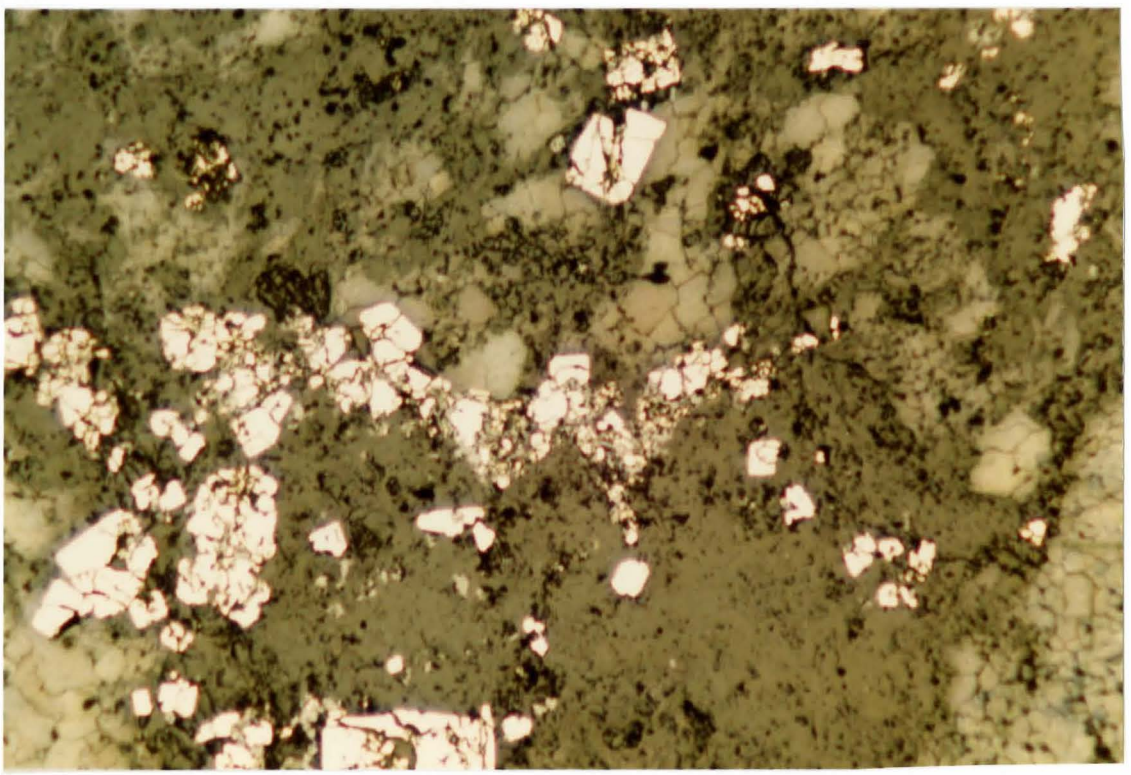

PLATE 3.8: Cataclastic deformation of pyrite. From M-415 under reflected light (20x).

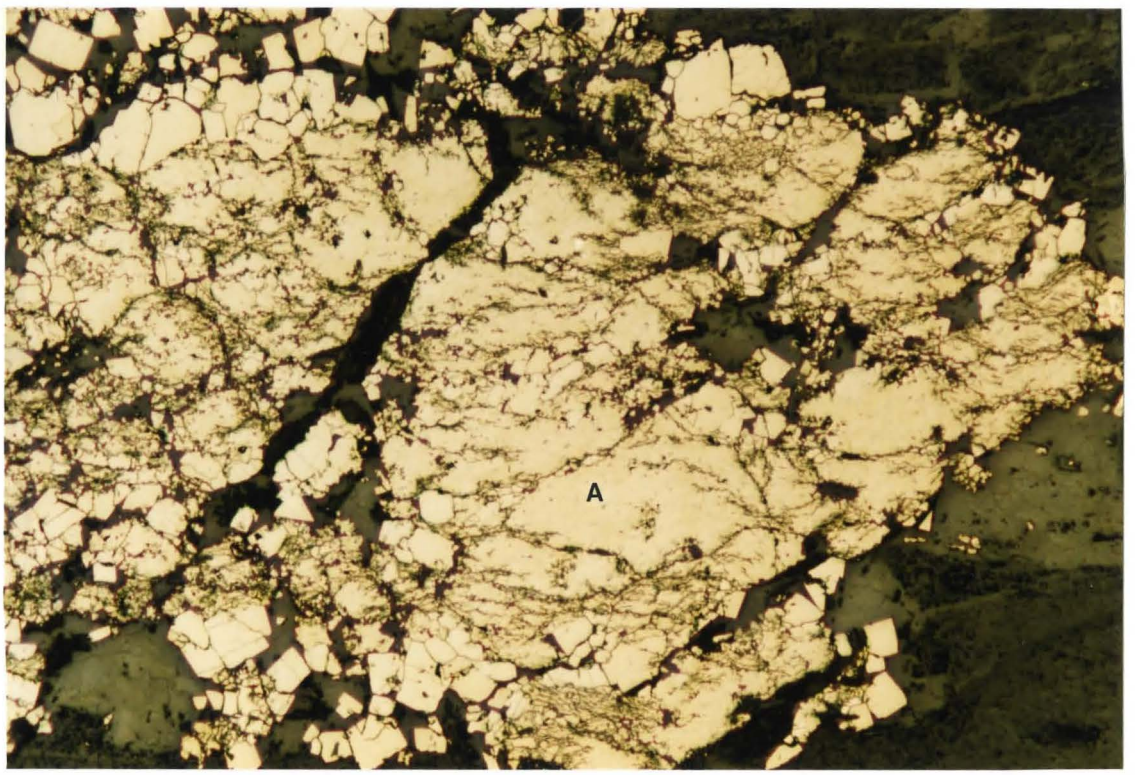

PLATE 3.9: Annealing recrystallization of fine grained pyrite (A). From M-755B under reflected light (20x).

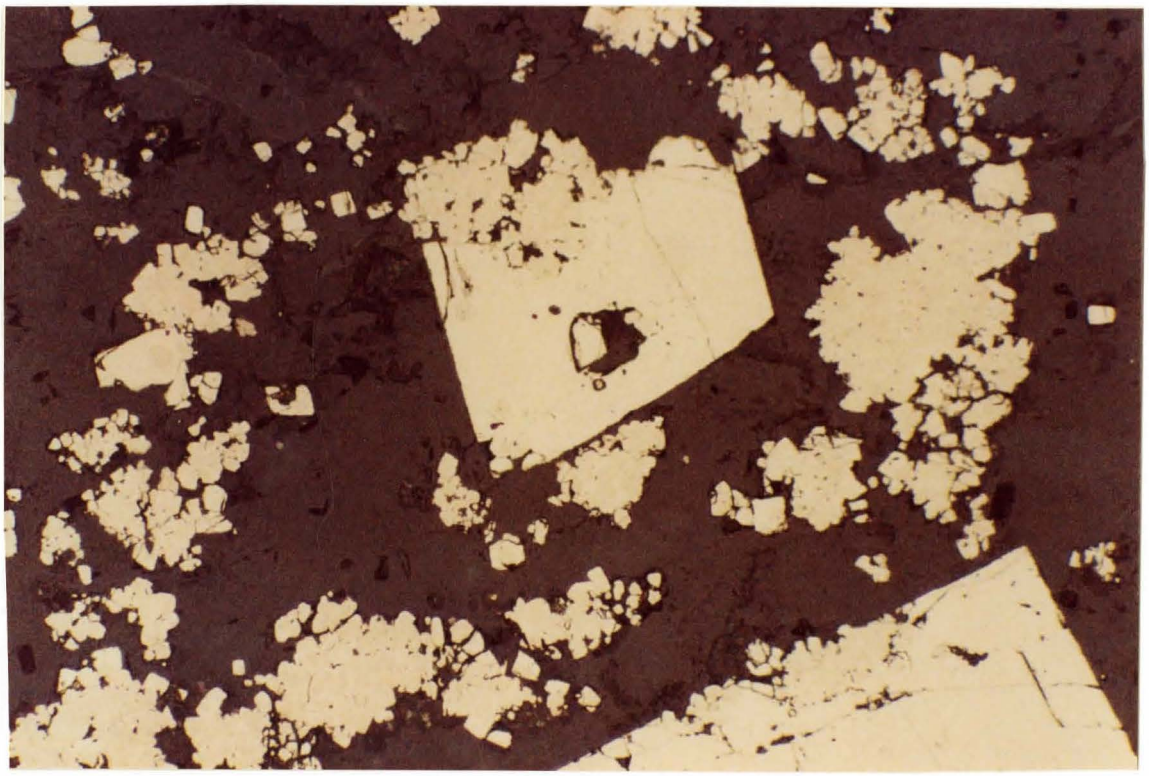

PLATE 3.10: Epitaxial growth of fine grained pyrite from cataclastic deformation fusing onto larger subhedral pyrite grains. From M-755B under reflected light (179x).

PLATE 3.11: Pyrite overgrowths (E) on subhedral pyrite (F). From M-408 under reflected light (64x).

annealing and subsequent recrystallization as seen in Plate 3.9. The presence of pyrite overgrowths may represent a second generation of pyrite (Py II) or possibly epitaxial growth of fine grained pyrite produced from cataclastic deformation onto the surface of subhedral to euhedral pyrite (Py I). Since this texture is only found in M-408, a definitive explantion for the pyrite overgrowths cannot be substantiated.

As previously mentioned, randomly oriented hydrothermal quartz veinlets are syn- or post-metamorphism. A second generation (mineralization II) of fracture controlled sulphide mineralization has been observed in these veinlets (see Plates 3.13 and 3.14).

A peculiar texture shown in Figures 3.12, 3.13 and 3.14 occurs in many of the slides. This texture is characterized by a colloidal and a poorly reflecting, fine grained core with a "corona" of sulphide around it. After fine polishing with 0.3 micron polishing powder, the colloidal outlines and core were discovered to be partly tarnished. But, the colloid type outlines and the cores were still detectable after re-polishing. The sulphide "coronas" have a paler or deeper yellow colour and also a lower relief than pyrite as shown in Plate 3.12. Also, the cores are usually slightly anisotropic while the coronas are isotropic. This, however, is not always the case as

the cores may also be isotropic (see Plate 3.14). Samples displaying this texture have relatively high Ni contents compared to the rest of the suite. The author proposes that the isotropic "coronas" and colloidal sulphides grains may be a secondary oxidizing Ni-rich mineral mineral or the development of a Ni-rich phase from pyrrhotite due to contact metamorphic effects. Further testing, such as microprobe analysis, is required before a certain mineral identification can be made. It should be noted, however, that this texture occurs both within fracture filled hydrothermal veins and throughout the host rock. Therefore, one may infer that the formation of the fracture controlled sulphides was possibly affected in part by contact metamorphism and was syn- or post-intrusion of the Lebel stock.

The remobilization of chalcopyrite is only found in M-419. The lack of remobilization is a reflection of the minor amounts of chalcopyrite present. Based on the previous discussion, the paragenetic sequence for the reflecting mineralogy is suggested in Figure 3.2.

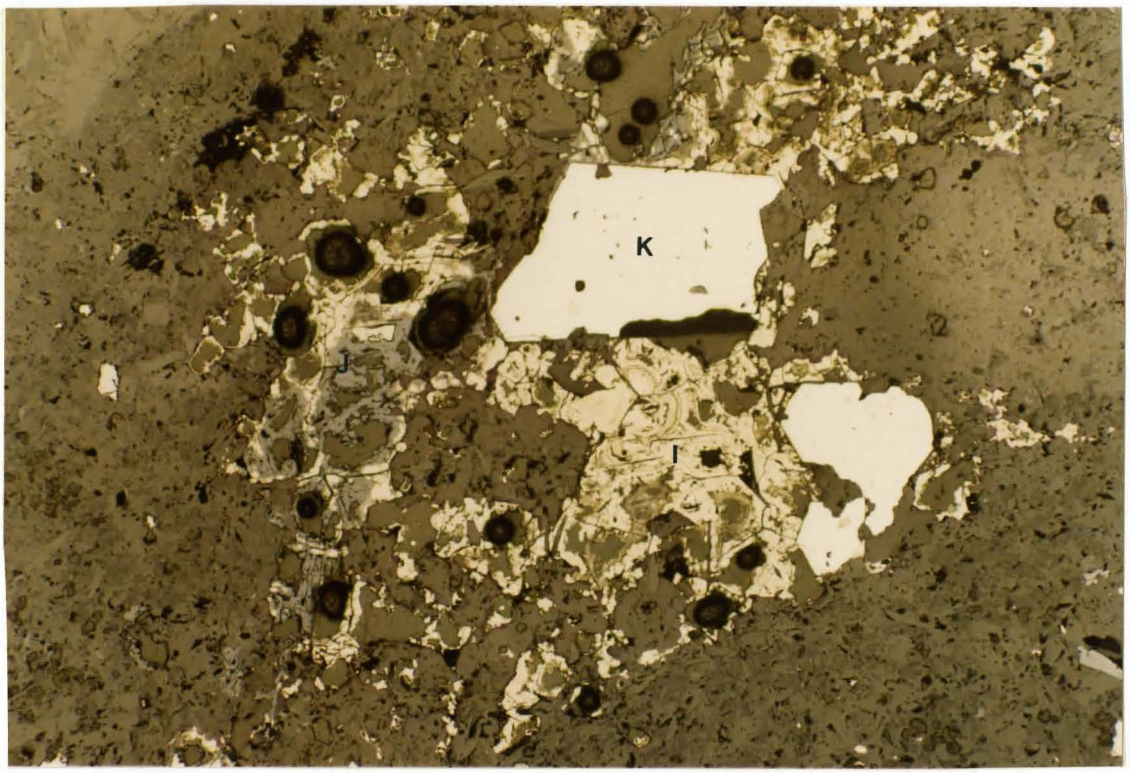

PLATE 3.12: Ni-rich corona-colloform textured assemblage (I) associated with hematite (J) and pyrite (K). Note the lower relief and paler yellow colour of the Ni-rich sulphide compared to the pyrite. From M-419 under reflected light (64x).

PLATE 3.13: Fracture controlled sphalerite (C) and pyrrhotite core (D) with possible Ni-rich corona (E). From M-320 under reflected (64x).

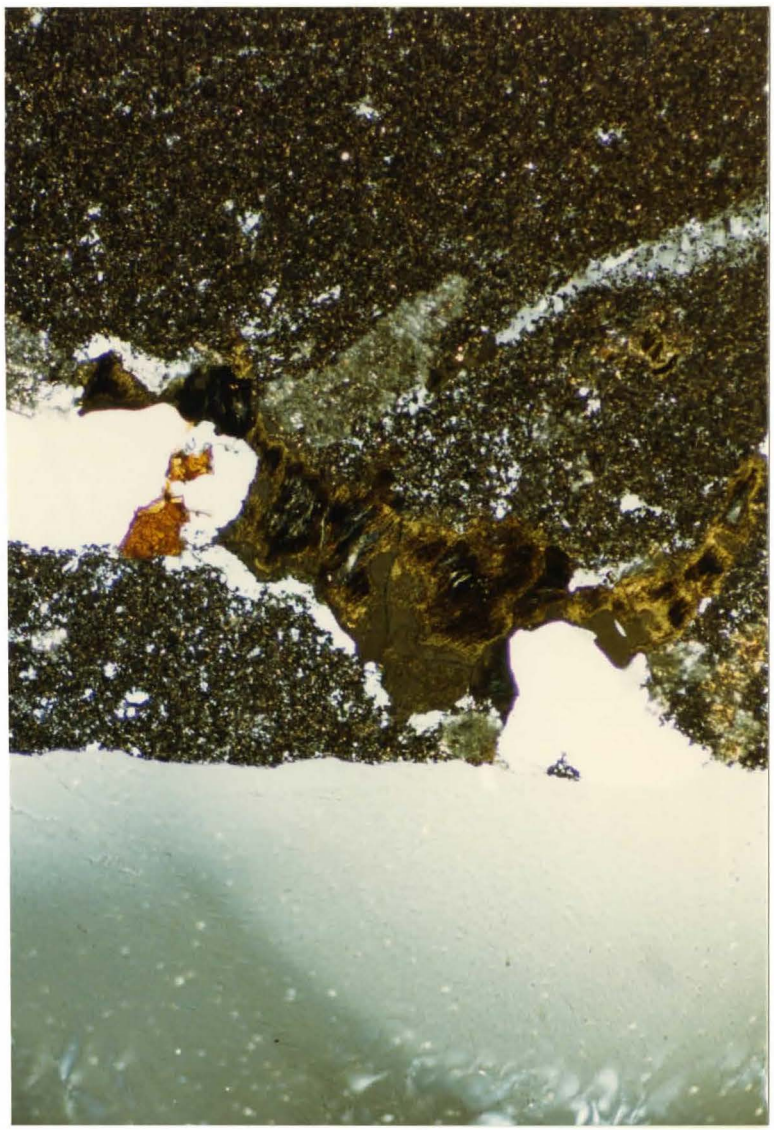

PLATE 3.14: Same frame as PLATE 3.13 except under reflected polarized light. The tarnished or reaction zone of the fine grained core is the bright yellow rimming the black core (64x).

FIGURE 3.2: Paragenesis based on reflected light mineralogy.

Legend:

I	First generation of mineralization.
II	Second generation of mineralization.
III	Third generation of mineralization.
Py	pyrite.
Po	pyrrhotite.
Cpy	chalcopyrite.
Mt	magnetite.
Cr	chromite.
Sph	sphalerite.

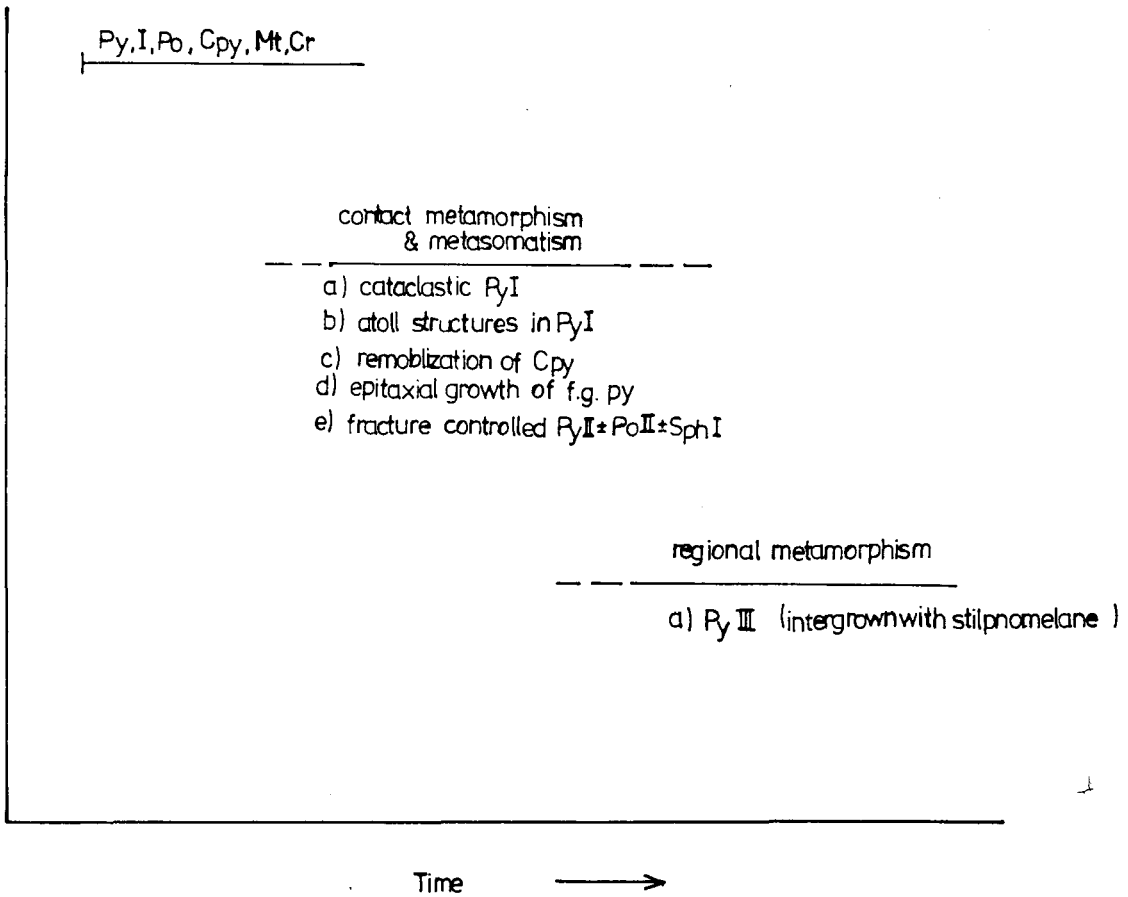
Py, I, Po, Cpy, Mt, Cr
contact metamorphism
& metasomatism
a) cataclastic PyI
b) atoll structures in PyI
c) remoblization of Cpy
d) epitaxial growth of f.g. py
e) fracture controlled PyII ± PoII ± SphI
regional metamorphism
a) Py III (intergrown with stilpnomelane)
Time

CHAPTER 4

GEOCHEMISTRY:

4.0 GEOCHEMICAL ANALYSIS:

The samples were analyzed by XRF for the major elements and sulphur. CO2 abundances were determined by LECO and an acid evolution-gravimetric method while LOI was determined by outgassing the sample in air at approximately 1000^{o} C. The results are displayed in Table 4.1. XRF was also used to determine the abundances of Cu, Pb, Zn, Ni, Co, Cr, and V, and Epithermal Instrumental Neutron Activation Analysis (EINAA) was used to determine the abundances of Au, As, W and Sb. These values are shown in Table 4.2. Refer to Appendix A for a detailed description of the experimental procedures and calculations.

4.1 GENERAL TRENDS:

The values in Tables 4.1 and 4.2 are compared to values from Bowins (unpublished data), Cameron and Garrels (1980) and Goodwin (1977). Bowins' values are for cherty, carbonaceous sediments taken from the Peria pit of the Adams Mine. The Peria pit is believed to be an eastward extension of the South pit economic BIF. These data were used to compare carbonaceous sediments from the economic

TABLE 4.1: Major element geochemical analysis. (by XRF)

Legend:

BOWINS- unpublished data from R. Bowins on carbonaceous cherts/shale from the Adams mine Peria pit.

CAM+GARR- data from Cameron and Garrels (1979).

MAT/LLK+K Matachewan and Larder Lake and Kenojevis Riveraverage values for 67 samples.

WGHDAVE Weighed average of 406 Archean shale samples.

GOODWIN- data from Goodwin (1980). Weighed average of extrusive volcanics in the Superior province.

* value determined experimentally by LECO.

	SAMPLE	SiO2(%)	Al2O3(%)	Fe2O3(%)	MgO(%)	CaO(%)	Na2O(%)	K2O(%)	TiO2(%)	MnO(%)	P2O5(%)	LOI(%)	SUM	S(%)	CO2(%)	Na2O/K2O
	M-320	65.52	7.70	2.94	0.64	1.23	0.30	6.98	0.27	0.05	0.07	14.30	100.00	10.06	0.15	0.04
	M-279	74.35	9.28	4.26	0.26	6.64	1.01	0.37	0.15	0.05	0.01	3.60	100.00	3.63	0.08	2.73
	M-647	77.70	11.77	1.96	0.24	1.31	2.08	3.92	0.17	0.02	0.03	0.80	100.00	0.28	*0.76	0.53
A	M-065	77.54	6.09	0.52	0.09	0.27	0.79	1.86	0.29	0.01	0.02	12.50	100.00	1.94	0.16	0.42
	M-781	91.24	3.05	0.89	0.02	0.53	1.08	0.54	0.12	0.00	0.02	2.50	100.00	0.86	*8.97	2.00
	M-755B	69.68	5.33	11.72	0.04	0.36	1.22	1.00	0.09	0.00	0.04	10.50	100.00	0.33	0.11	1.22
	M-146	72.89	13.63	3.11	1.10	1.97	3.93	1.79	0.25	0.04	0.08	1.20	100.00	3.26	0.00	2.20
	M-408	66.88	15.40	5.60	1.38	1.81	3.84	2.51	0.26	0.05	0.04	2.20	100.00	5.05	0.12	1.53
	M-784	73.12	2.05	12.66	0.14	5.89	0.35	0.24	0.07	0.26	0.01	5.20	100.00	12.01	0.42	1.46
	M-419	39.43	5.67	32.66	4.20	7.85	0.96	0.90	0.35	0.36	0.02	7.60	100.00	19.77	0.11	1.07
	M-415	77.92	2.55	12.67	0.18	3.02	0.23	0.06	0.11	0.11	0.03	3.10	100.00	5.90	0.12	3.83
	M-774	58.69	5.99	20.58	2.34	0.20	0.18	0.44	0.20	0.14	0.13	11.10	100.00	13.20	0.14	0.41
	M-775A	54.08	7.49	16.74	0.54	0.31	1.32	1.53	0.15	0.00	0.03	17.80	100.00	21.75	0.12	0.86
B	M-770	76.25	13.11	0.96	0.19	0.47	1.12	5.81	0.13	0.00	0.05	1.90	100.00	0.33	*3.16	0.19
	M-771	73.02	15.52	2.33	0.56	1.13	1.35	4.54	0.20	0.02	0.03	1.30	100.00	0.08	*0.45	0.30
	M-772	71.38	15.53	1.09	0.50	4.29	3.25	2.68	0.25	0.06	0.17	0.80	100.00	0.51	*0.14	1.21
	M-773	75.68	13.39	2.21	0.52	0.68	5.35	1.21	0.26	0.02	0.08	0.60	100.00	0.31	*0.07	4.42
	M-780	83.85	8.97	1.19	0.06	1.64	2.83	0.75	0.23	0.03	0.05	0.40	100.00	0.10	*0.19	3.77
	M-783	56.23	16.38	9.34	3.42	5.48	4.69	1.38	0.74	0.26	0.18	1.90	100.00	4.14	0.19	3.40
	M-130	70.28	14.77	4.87	0.83	1.63	3.07	2.50	0.44	0.07	0.13	1.40	100.00	0.81	*0.77	1.23
	M-089	73.22	9.60	5.99	0.17	3.80	3.01	2.36	0.27	0.12	0.07	1.40	100.00	1.81	0.77	1.28
	M-319	62.87	10.44	11.31	1.85	5.96	3.57	0.55	0.33	0.13	0.20	2.80	100.00	8.13	0.18	6.49
C	M-143	72.56	14.53	2.10	0.25	4.76	2.76	1.81	0.28	0.07	0.06	0.80	100.00	0.76	*1.00	1.52
	M-211	48.69	13.24	12.48	2.57	1.68	4.55	1.52	0.30	0.06	0.11	14.80	100.00	13.48	0.10	2.99
	M-592	45.81	9.56	22.00	1.11	1.68	2.45	1.33	0.24	0.06	0.06	15.70	100.00	23.24	0.08	1.84
	DUPLICATE															
	M-211	48.91	13.15	12.30	2.68	1.74	4.35	1.61	0.32	0.06	0.07	14.80	100.00	13.53	0.08	2.70
	M-781	92.04	2.65	0.53	0.05	0.40	1.13	0.56	0.12	0.00	0.02	2.50	100.00	1.03	*8.82	2.02
	M-784	74.30	1.93	11.50	0.10	6.02	0.34	0.24	0.08	0.25	0.02	5.20	100.00	9.75	0.26	1.42
	M-130															
	M-419															
	M-592															
	BOWINS															
	P11C1	54.05	12.48	19.99	4.30	0.71	0.00	6.00	0.53	0.13	0.10		98.29			
	P12	39.30	3.97	38.05	7.97	7.28	0.33	1.89	0.18	0.79	0.25		99.99			
	KLGS	58.13	5.22	17.72	0.64	6.17	0.00	1.48	0.18	0.08	0.09		89.71			
	P13C															
	CAM+GARR															
	MAT/LLK+K	57.50	18.40	8.10	3.83	1.39	2.50	3.20	0.83	0.09	0.19	4.40		0.14	0.90	
	WGHDAVE	58.00	16.90	7.60	3.33	2.07	2.50	2.73	0.73	0.09	0.16	4.50		0.66	1.10	
	GOODWIN															
	BASALT	49.10	14.60	11.20	6.20	8.90	2.62	0.51	1.15	0.21	0.14	3.30			1.17	
	ANDESITE	55.10	15.90	7.90	4.30	5.90	3.85	1.14	0.96	0.17	0.20					
	DACITE	66.90	15.40	4.40	1.90	2.70	4.20	1.30	0.50	0.10	0.10					
	RHYOLITE	74.20	13.30	8.10	0.80	0.80	3.70	2.10	0.30	0.10	0.10					

TABLE 4.2: Trace Element Geochemical Analysis (by EINAA and XRF)

LEGEND: same as Table 4.1

	SAMPLE	Au(ppb)	As(ppm)	W(ppm)	Sb(ppm)	Cu(ppm)	Pb(ppm)	Zn(ppm)	Ni(ppm)	Co(ppm)	Cr(ppm)	V(ppm)
	M-320	12.52	693.12	2.20	5.31	290.00	15.00	2934.00	137.00	163.00	71.00	41.00
	M-279	5.07	0.79	0.24	0.35	66.00	18.00	1684.00	134.00	46.00	420.00	31.00
	M-647	4.34	1.72	0.47	0.14	11.00	14.00	46.00	7.00	2.00	283.00	8.00
A	M-065	0.39	23.38	0.47	0.35	4.00	15.00	19.00	13.00	9.00	100.00	36.00
	M-781	3.37	6.32	0.54	0.16	53.00	15.00	944.00	27.00	42.00	20.00	2.00
	M-755B	36.04	85.35	0.39	6.33	7.00	12.00	95.00	17.00	21.00	318.00	4.00
	M-146	0.34	0.70	0.00	0.07	52.00	24.00	342.00	78.00	39.00	387.00	60.00
	M-408	2.36	12.43	1.20	0.34	42.00	13.00	242.00	44.00	20.00	321.00	62.00
	M-784	1.15	8.93	1.26	0.18	38.00	8.00	251.00	130.00	21.00	31.00	16.00
	M-419	4.22	2.28	0.88	0.01	231.00	11.00	176.00	1235.00	72.00	1744.00	94.00
	M-415	7.18	0.77	1.71	0.08	84.00	10.00	118.00	47.00	17.00	392.00	12.00
	M-774	9.49	9.74	0.78	0.63	28.00	12.00	156.00	149.00	86.00	52.00	57.00
	M-775A	30.68	147.27	1.17	7.03	10.00	11.00	127.00	96.00	25.00	26.00	17.00
B	M-770	2.87	3.67	0.22	0.17	9.00	31.00	52.00	7.00	4.00	251.00	10.00
	M-771	3.62	0.83	0.77	0.11	34.00	20.00	109.00	10.00	6.00	259.00	19.00
	M-772	0.34	1.40	0.51	0.07	11.00	17.00	20.00	7.00	3.00	193.00	36.00
	M-773	1.69	0.86	0.16	0.00	43.00	13.00	116.00	11.00	8.00	255.00	45.00
	M-780	1.06	693.12	0.10	0.08	11.00	13.00	48.00	13.00	6.00	101.00	58.00
	M-783	5.14	2.69	1.71	0.08	33.00	13.00	141.00	64.00	19.00	105.00	119.00
	M-130	3.32	14.66	0.71	0.24	34.00	36.00	125.00	24.00	15.00	301.00	59.00
	M-089	2.54	3.07	3.98	1.34	112.00	47.00	168.00	30.00	27.00	242.00	70.00
	M-319	4.38	0.89	0.90	0.00	223.00	13.00	231.00	147.00	72.00	44.00	56.00
C	M-143	3.62	6.75	0.31	0.06	26.00	12.00	69.00	18.00	12.00	61.00	63.00
	M-211	10.09	35.71	1.97	0.25	56.00	14.00	72.00	84.00	53.00	46.00	53.00
	M-592	5.59	12.80	0.00	0.42	288.00	12.00	181.00	198.00	49.00	78.00	41.00
	DUPLICATE											
	M-211					66.00	12.00	73.00	82.00	48.00	48.00	47.00
	M-781					55.00	12.00	890.00	20.00	29.00	55.00	4.00
	M-784					40.00	8.00	67.00	83.00	13.00	54.00	13.00
	M-130	3.26	10.19	0.03	0.27							
	M-419	4.24	2.65	1.05	0.10							
	M-592	7.65	14.76	1.05	0.27							
	BOWINS											
	P11C1					48.00	7.00	123.00	82.00	10.00	185.00	77.00
	P12	16.95	1.80	73.42	0.17	480.00	3.00	357.00	155.00	52.00	15.00	39.00
	KLGS	489.00	188.25	2.21	4.15	92.00	15.00	424.00	114.00	35.00	127.00	39.00
	P13C	16.95	1.80	73.42	0.17							
	CAM+GARR											
	MAT/LLK+K		61.00		0.70	52.00	16.00	114.00	140.00	35.00	168.00	150.00
	WGHDAVE		46.00		1.20	66.00	26.00	323.00	127.00	35.00	133.00	130.00
	GOODWIN											
	BASALT					106.00	3.90	81.00	170.00	36.00	245.00	372.00
	ANDESITE					64.00	8.10	77.00	55.00	29.00	105.00	231.00
	DACITE					32.00	6.70	71.00	21.00	11.00	22.00	83.00
	RHYOLITE					33.00	7.20	44.00	14.00	11.00		49.00

BIF and those analyzed from the study area. Generally, the economic BIF carbonaceous sediments have higher Au, W, and Cu values but lower Pb and Cr values. Also, the economic BIF samples have higher Fe2O3 abundances compared to the thesis area samples. The higher Fe2O3 content in Bowins' samples may be attributed to the greater percentage of Fe-sulphides (pyrite + pyrrhotite + arsenopyrite) present (up to approximately 35% sulphide in the KLGS hand sample) or else leaching from the BIF. Also, Bowins' samples generally have a lower Na2O/K2O ratio than the carbonaceous thesis samples. This may be attributed to the occurrence of albite in the study samples.

Two sets of geochemical data have been listed from Cameron and Garrels (1980) in Tables 4.1 and 4.2. The first set of data represents an average of 67 shale samples from the Matachewan and Larder Lake and Kenojevis River region. The second set of data is a compositional weighted average of 406 samples from Archean shales in the Superior province. The main purpose of these two sets of data is to provide a general compositional average with which to compare the study samples.

M-419 is different from other samples due to the relatively low SiO2 content and high Ni, Cr, Fe and MgO contents. The MgO content of M-419, however, is too low to be considered a komatiite or basaltic komatiite as these

types of rocks have 18% and 10% MgO respectively (Viljoen and Viljoen, 1969). Also, the SiO2 content of M-419 is too low to be considered a basalt (see Goodwin values in Tables 4.1 and 4.2). Therefore, this rock may possibly be an Fe-rich component of the silicate facies BIF (Fyon, personal communication). The high Ni abundance may be due to the assumed Ni-rich corona-colloform textured assemblage discussed in Chapter 3 or the metamorphic diffusion of Ni from surrounding ultramafic rocks into the sulphide- rich metasediments (Groves et al., 1980).

4.2 BASE METAL ANALYSIS:

From the Ni-Cu-Zn ternary diagram in Figure 4.1, the samples tend to be enriched in Zn and generally depleted in Cu and Ni. Data points for this plot were calculated in weight percent and then normalized to 100%. The carbonaceous samples show the strongest enrichment in Zn while M-419 lies in the Ni-rich field. M-320, M-279 and M-781 are significantly enriched with Zn compared to the averages from Cameron and Garrels (1980). Sphalerite occurs mainly as a fracture controlled mineral (Table 3.2; also see Plates 3.13 and 3.14) and is probably due to mobilization of Zn and S during metasomatism. The higher Ni content samples found within the suite (ie. > 130 ppm) are usually associated with high Co contents (as in Figure

4.2) and the occurrence of the corona-colloidal textured mineral assemblage. But, this is not always the case as in M-783 and M-592 where, as stated earlier, the relatively high Ni contents may be due to the development of a Ni-rich phase from pyrrhotite due to contact metamorphic effects. Ni may also be associated with spheroidal and colloform pyrite and pyrrhotite in carbonaceous sediments of the Abitibi greenstone belt (Coad, 1979; Muir and Comba, 1979).

4.3 PRECIOUS METAL ANALYSIS:

Background values for Au in the continental crust is 4 ppb (Taylor, 1964). Therefore, samples with Au abundances > 10 ppb have been designated as samples having anomalous Au concentrations. This statement is made as a relative comparison with respect to background values. Samples with high Au contents occur in all three classes defined earlier (ie. CCS, NCS and CS).

Binary plots of major and trace elements against Au were performed to assist in defining possible trends. The lines for these plots were derived by linear regression and tested statistically at the 95% significance level. The solid line plots indicate that there is a significant correlation between Au and that particular element at the 95% confidence level. The dashed line plots indicate that there is no significant correlation at the 95% confidence

FIGURE 4.1: Ni-Cu-Zn Ternary Plot.

Legend:

- ✕ Carbonaceous chemical sediments.
- ⊘ Non-carbonaceous chemical sediments.
- ▽ Clastic sediments.

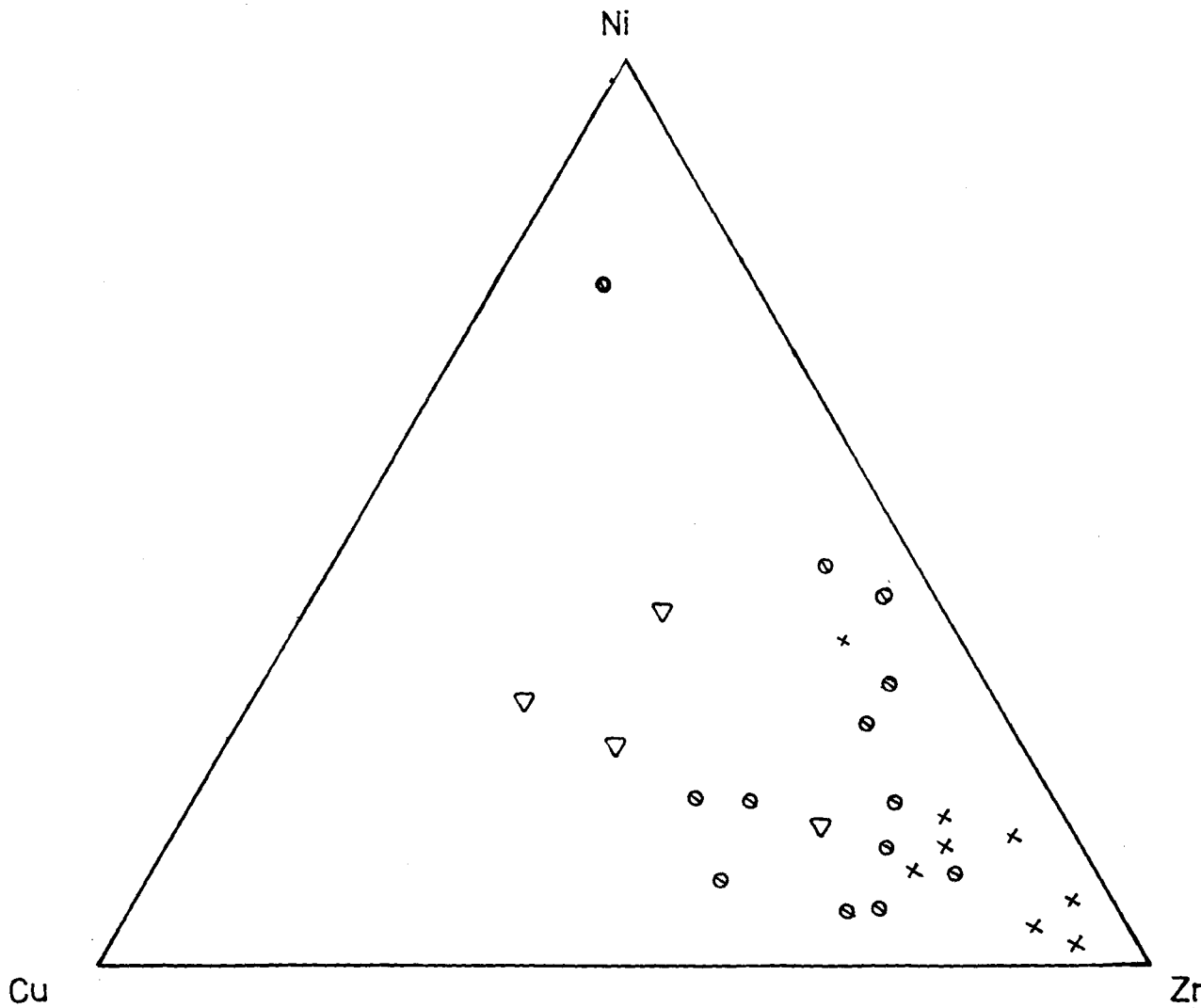
Ni
Cu
Zr

Figure 4.2: Co (ppm) vs. Ni (ppm)

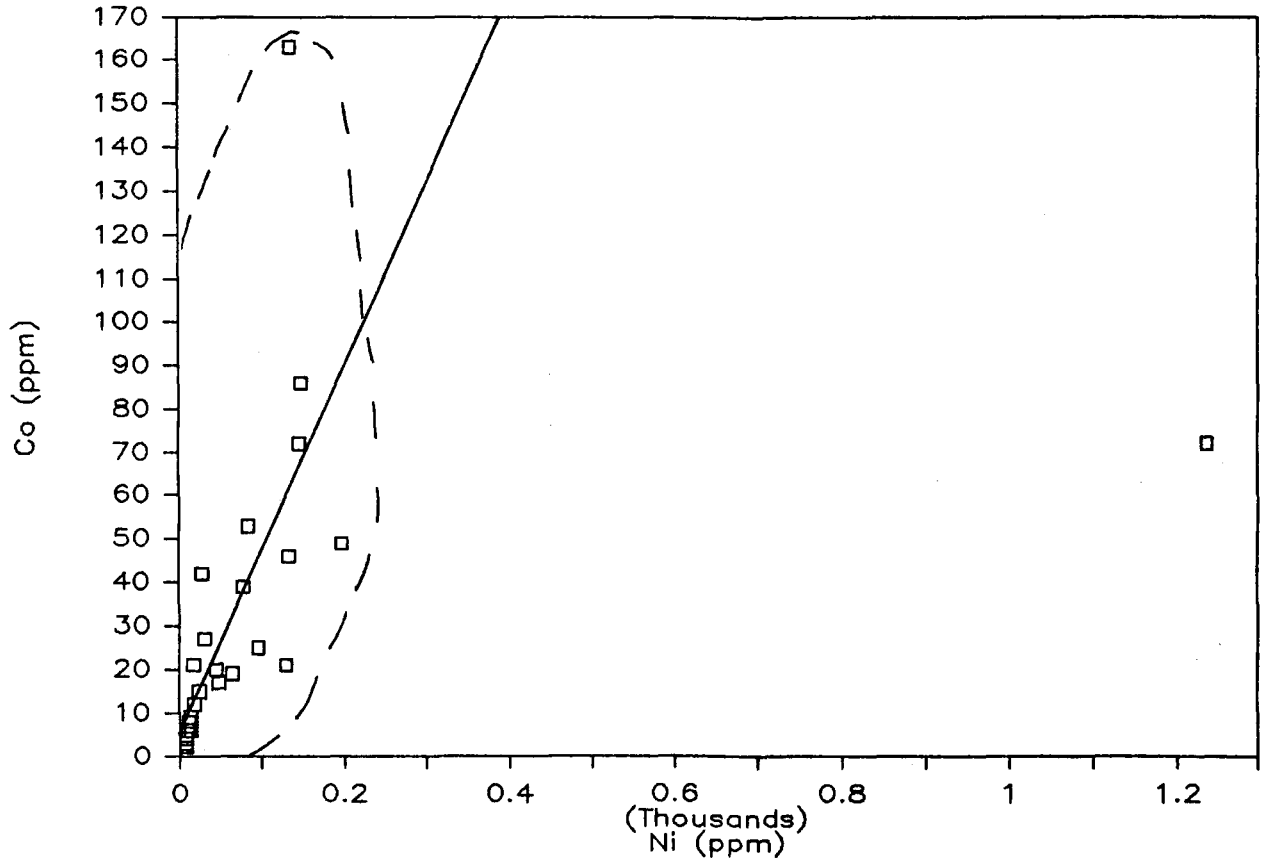

level. A sample calculation may be found in Appendix B.

4.3.1 MAJOR ELEMENT TRENDS WITH Au:

Au abundances above 10 ppb in the suite are characterized by low Al2O3 (see Figure 4.3) and MgO (see Figure 4.4) and high Fe2O3 and S contents (see Figure 4.5 and 4.6 respectively). The low Al2O3 association to Au implies the absence, or low modal percentages, of micas, hornblende and/or feldspar.

The association of high Au with high Fe2O3 and low Mgo abundances implies that the Au is not related to the mafic component of the rock, but more likely the sulphide mineralization. Pyrite and pyrrhotite are the most commonly intergrown sulphides with Au in Archean deposits (Colvine et al., 1984). Above background Au values may be due to pyrite and/or pyrrhotite acting as control sites for the Au. Wells and Mullens (1973) and Hausen (1981) have noted that the Au content of pyrite at the Carlin Mine varies with pyrite morphology. They found that fine grained spheroidal aggregates of pyrite yield the highest Au values, rims or overgrowths of pyrite around euhedral pyrite yield intermediate Au values and the euhedral crystals of pyrite yield the lowest values. This scheme may be applied to the study area as there is a possible

Figure 4.3: Al2O3 (Wt%) vs. Au (ppb)

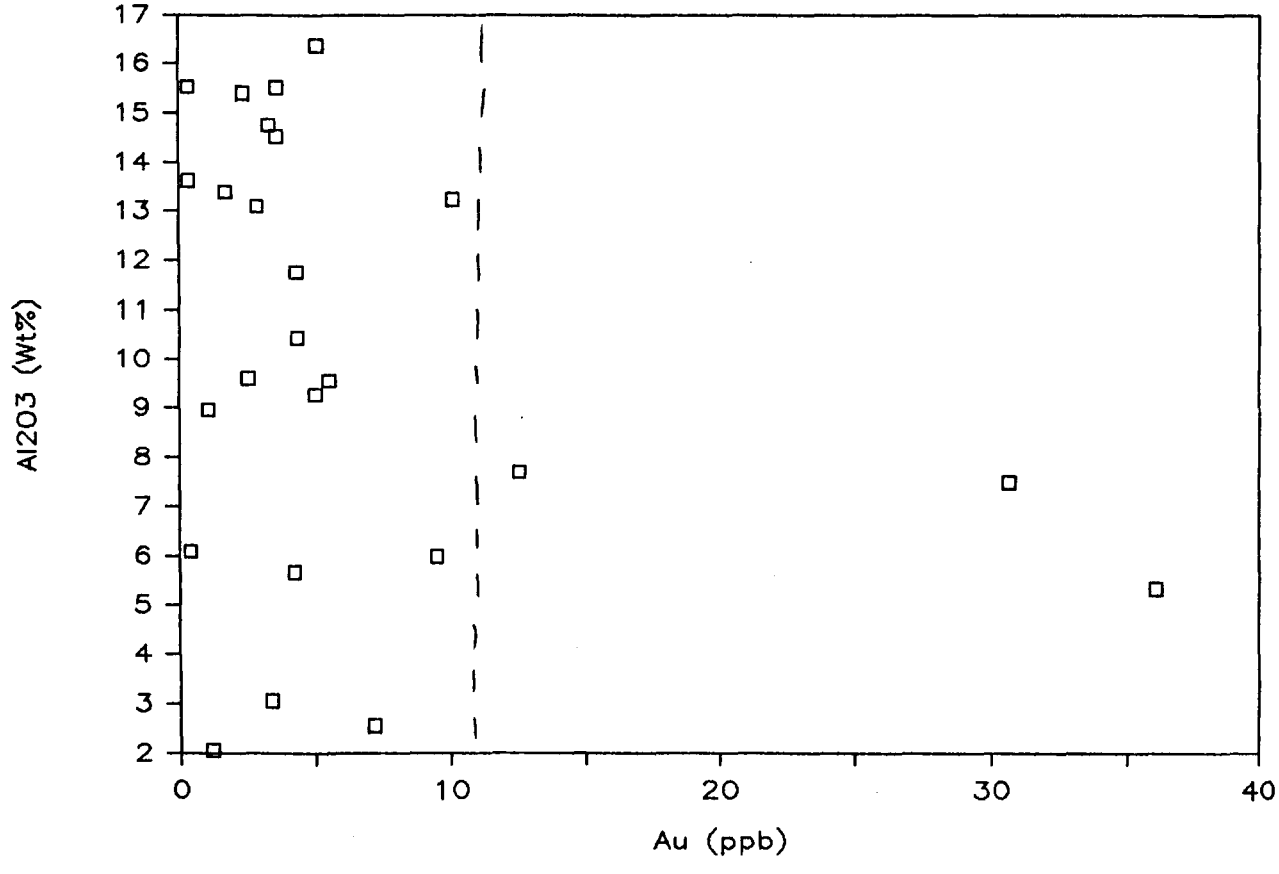

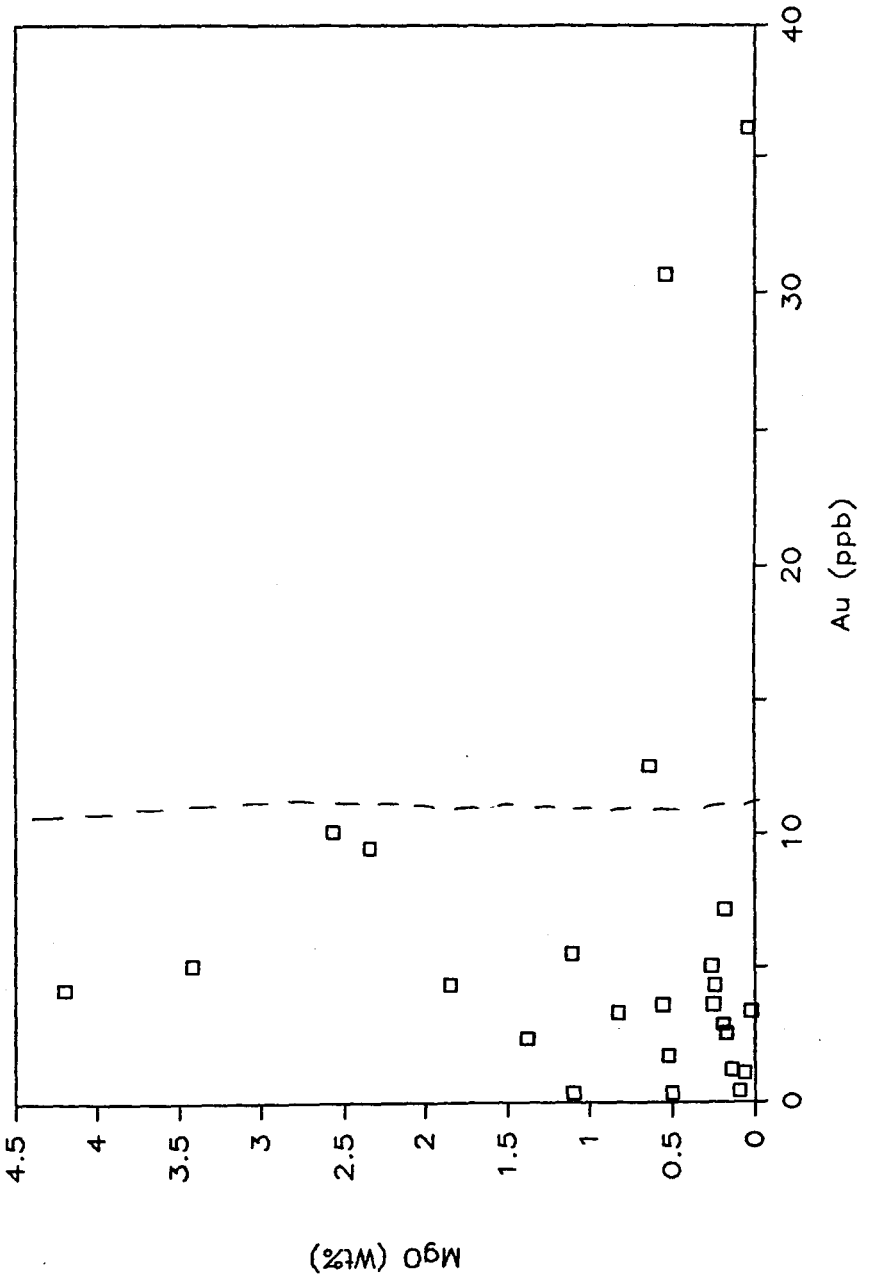

Figure 4.4:

Figure 4.5: Fe203(w%) vs. Au(ppb)

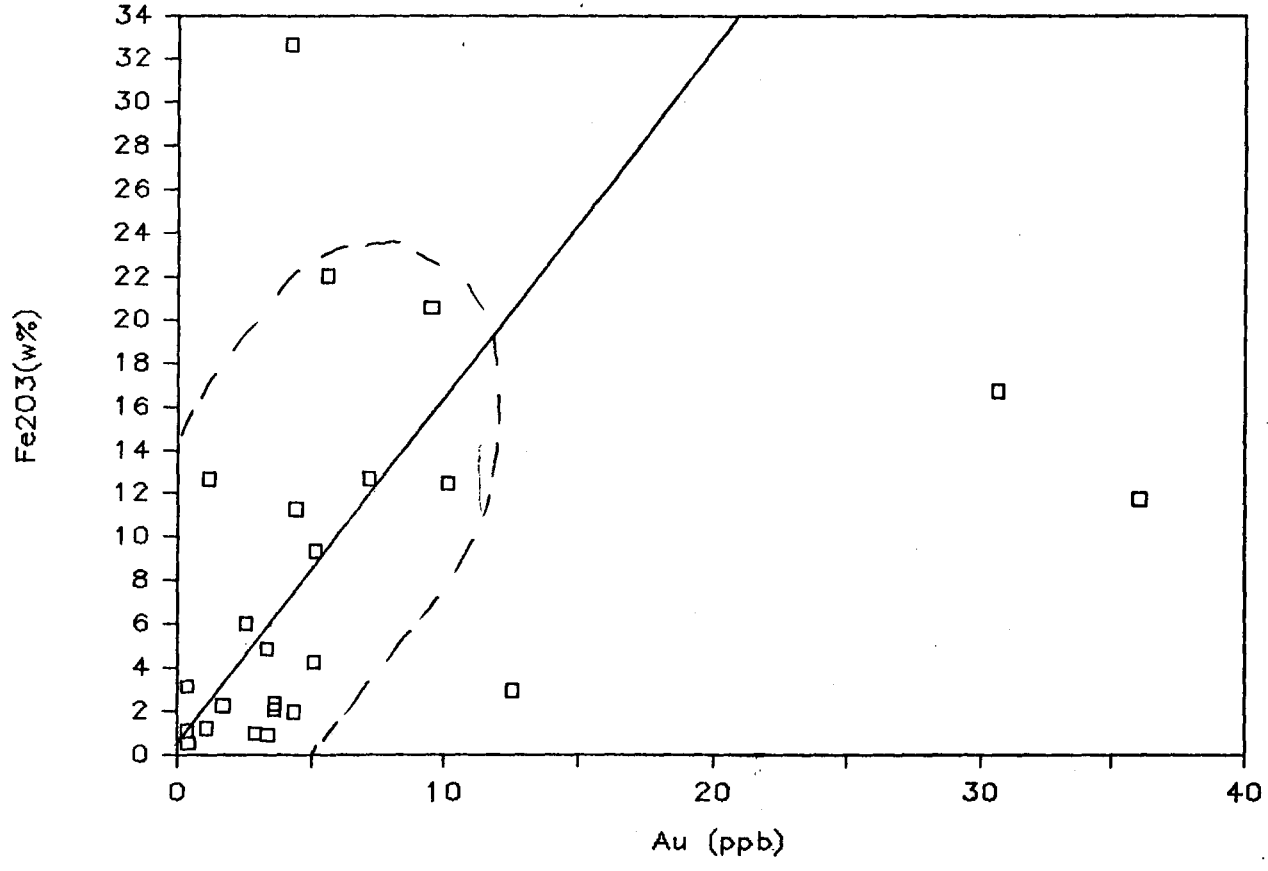

Figure 4.6:

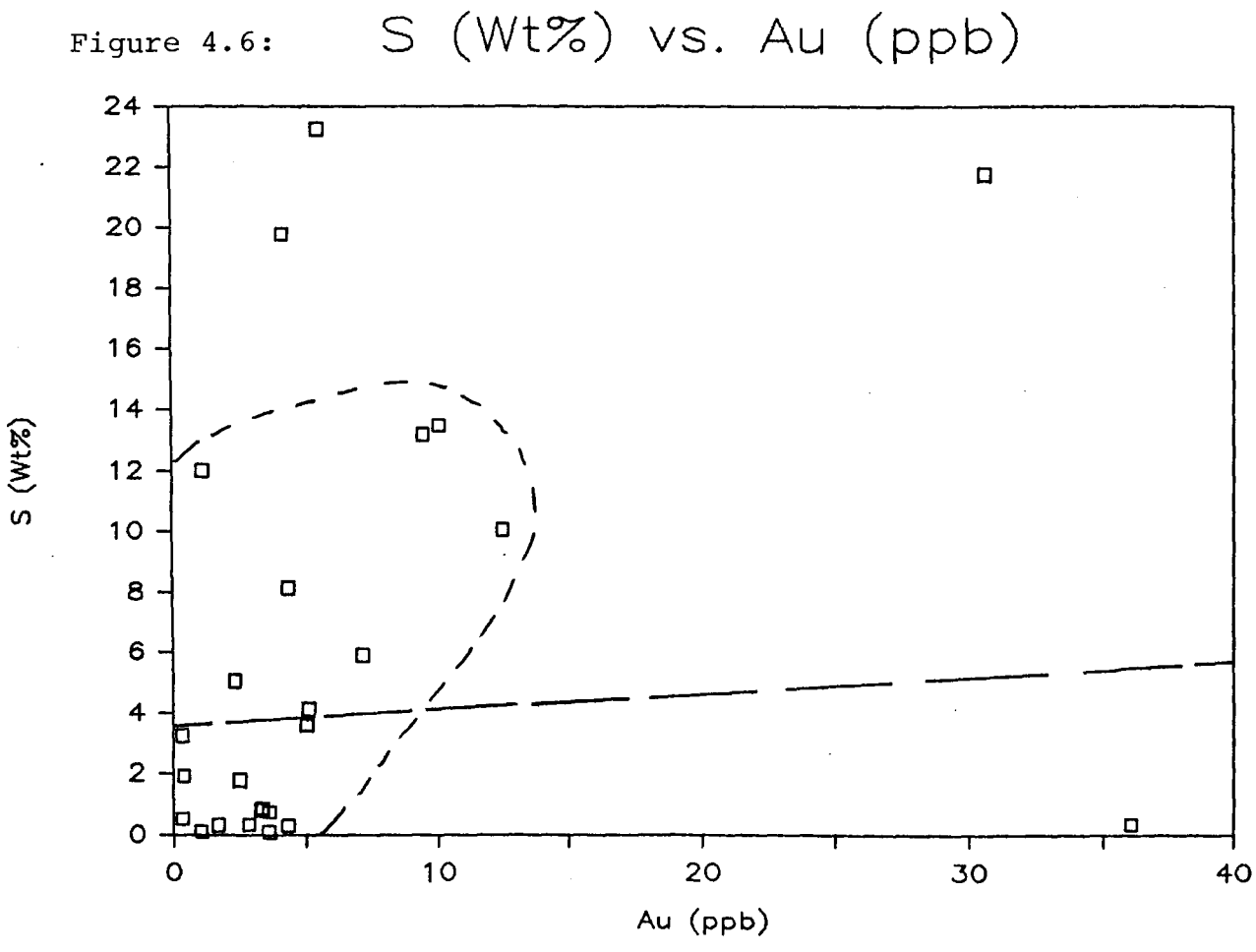

correlation between Au and fine grained pyrite aggregates formed from cataclastic deformation and subsequent annealing recrystallization (see Table 3.2). This also implies that Au deposition was synchronous with or post deformation of the area. There does not seem to be any correlation between pyrite overgrowths and Au abundance in the suite.

Except for M-320, high Au values are usually associated with modal percentages > 10% for pyrite. But, the same can not be said for the converse. The high Au abundance in M-320 and M-755B may be attributed in part to the adsorptive properties of activated organic/inorganic carbon (Wilson, 1985). Active carbon is capable of reducing Au complexes, such as AuCl or Au(HS)2 inducing the precipitation of free Au (Colvine et al., 1984: Wilson, 1985).

4.3.2 TRACE ELEMENT ASSOCIATIONS WITH Au:

Au is not statistically correlated with Sb and As (Figures 4.7 and 4.8 respectively). But, anomalous Au values usually coincide with values of > 85 ppm As and > 5 ppm Sb. The clastic sediment M-211 does not follow this trend completely as it is depleted in Sb and has a relatively low As concentration.

W and Zn were calculated to have significant positive correlations with Au (Figures 4.9 and 4.10 respectively). This is not surprising as Au may be associated with chalcopyrite, molybdenum and sphalerite (Colvine et al., 1984). If the Au is genetically linked with Zn, then the Au may quite possibly be related to the intrusion of the Lebel stock and the subsequent metasomatic processes associated with contact metamorphism. A word of caution should be noted as anomalous Au values are not always associated with high Zn values. The same is true for the converse. Cu produces a scatter diagram (Figure 4.11) and is not statistically correlated with Au.

Figure 4.7:

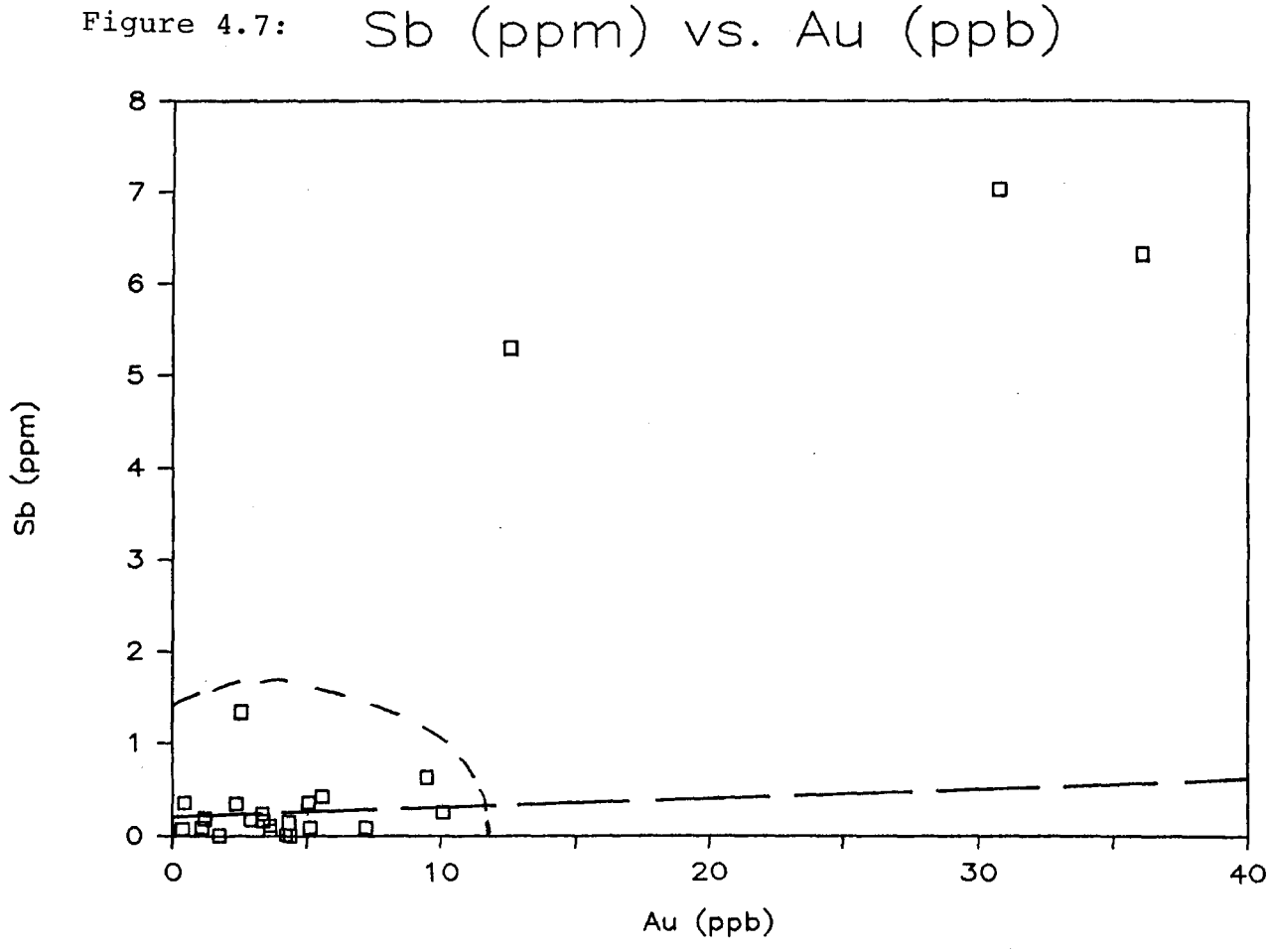

Figure 4.8: As (ppm) vs. Au (ppb)

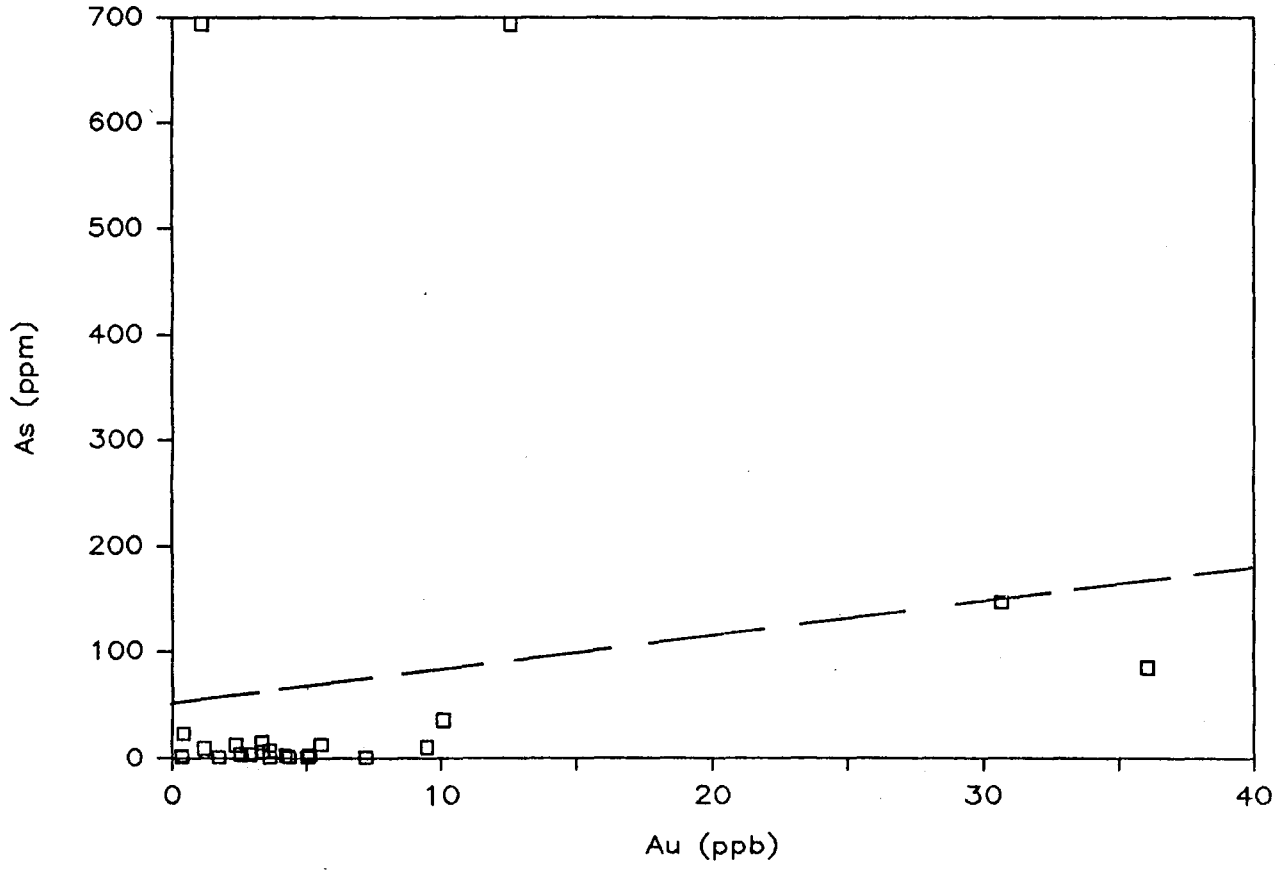

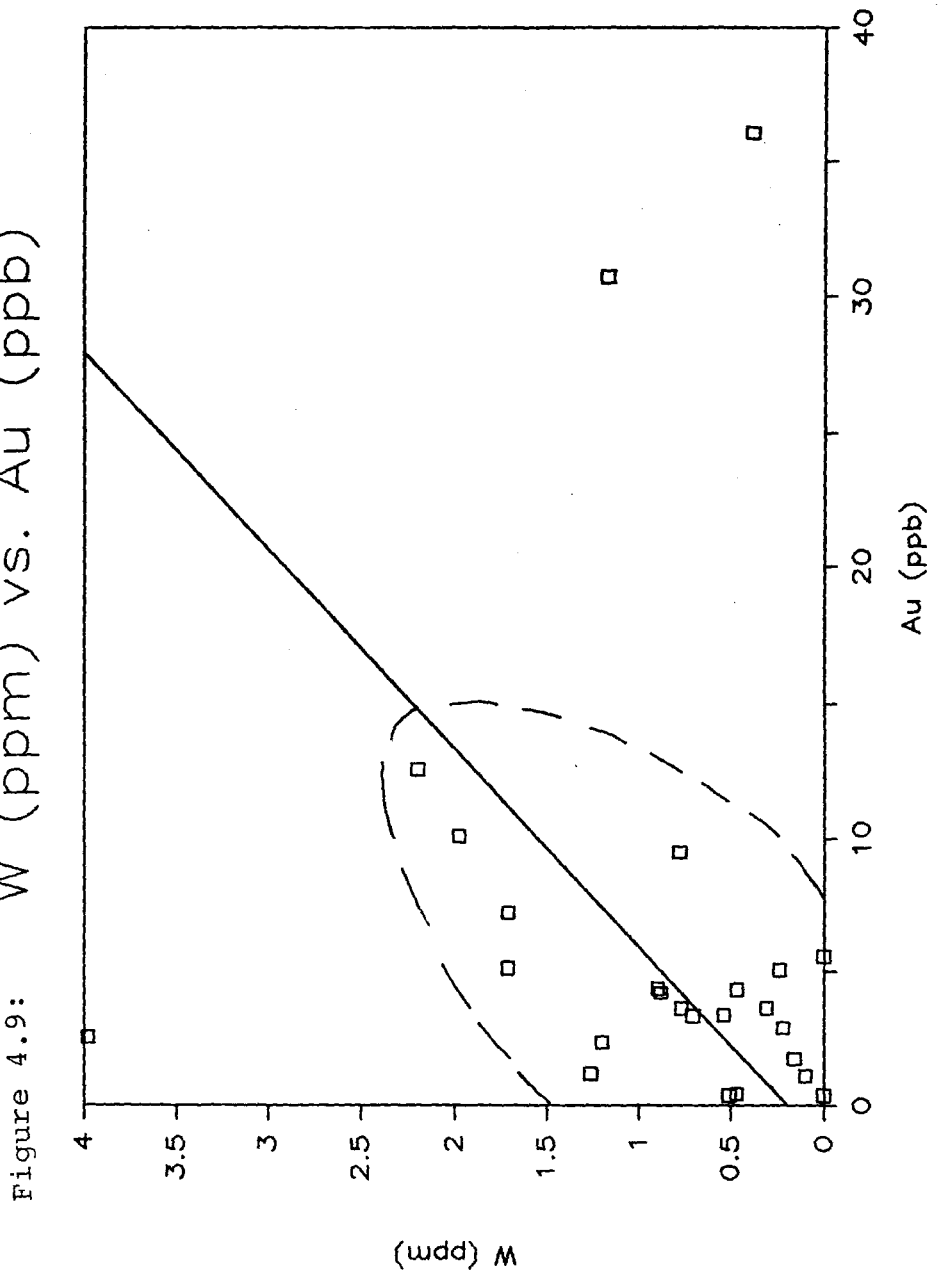

Figure 4.9:

Figure 4.10: Zn (ppm) vs. Au (ppb)

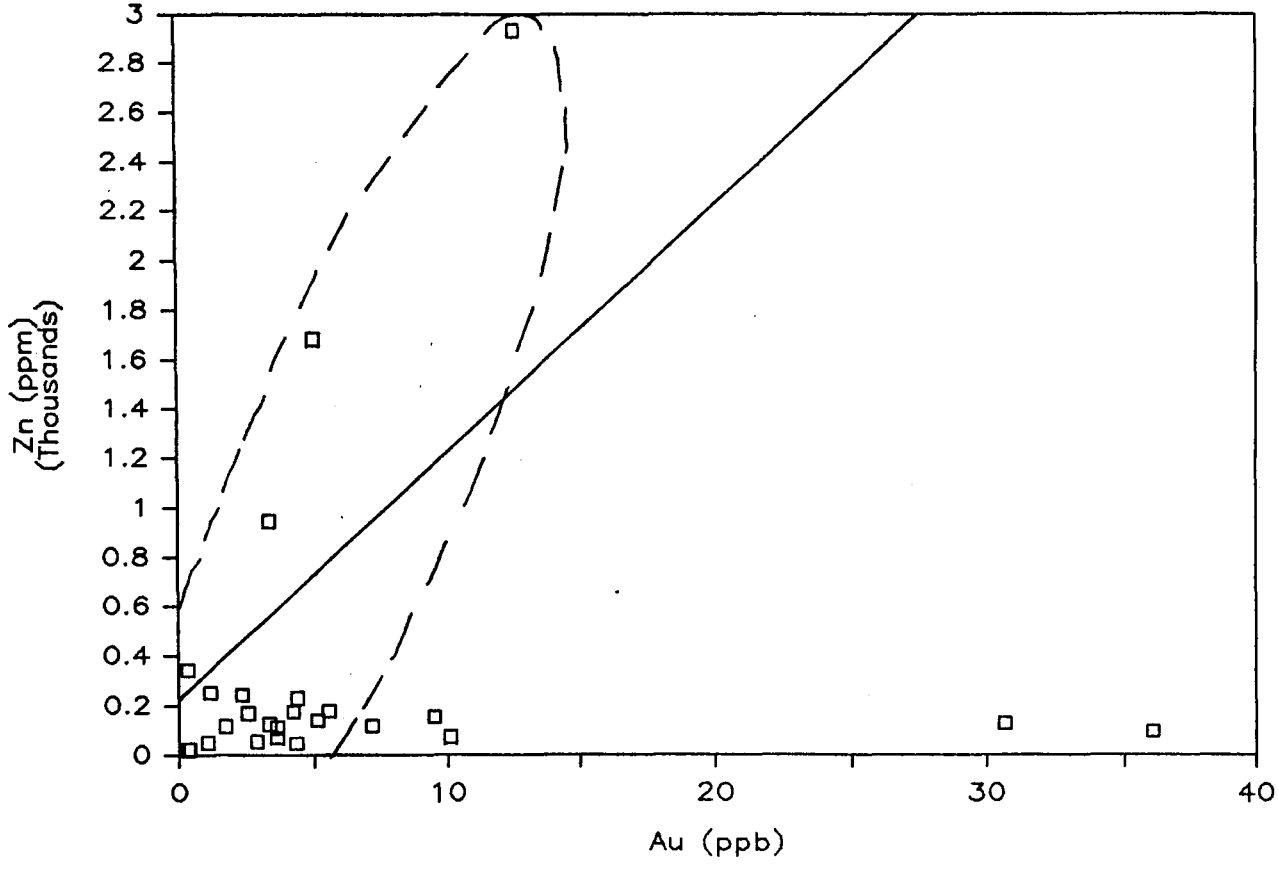

Figure 4.11: Cu (ppm) vs. Au (ppb)

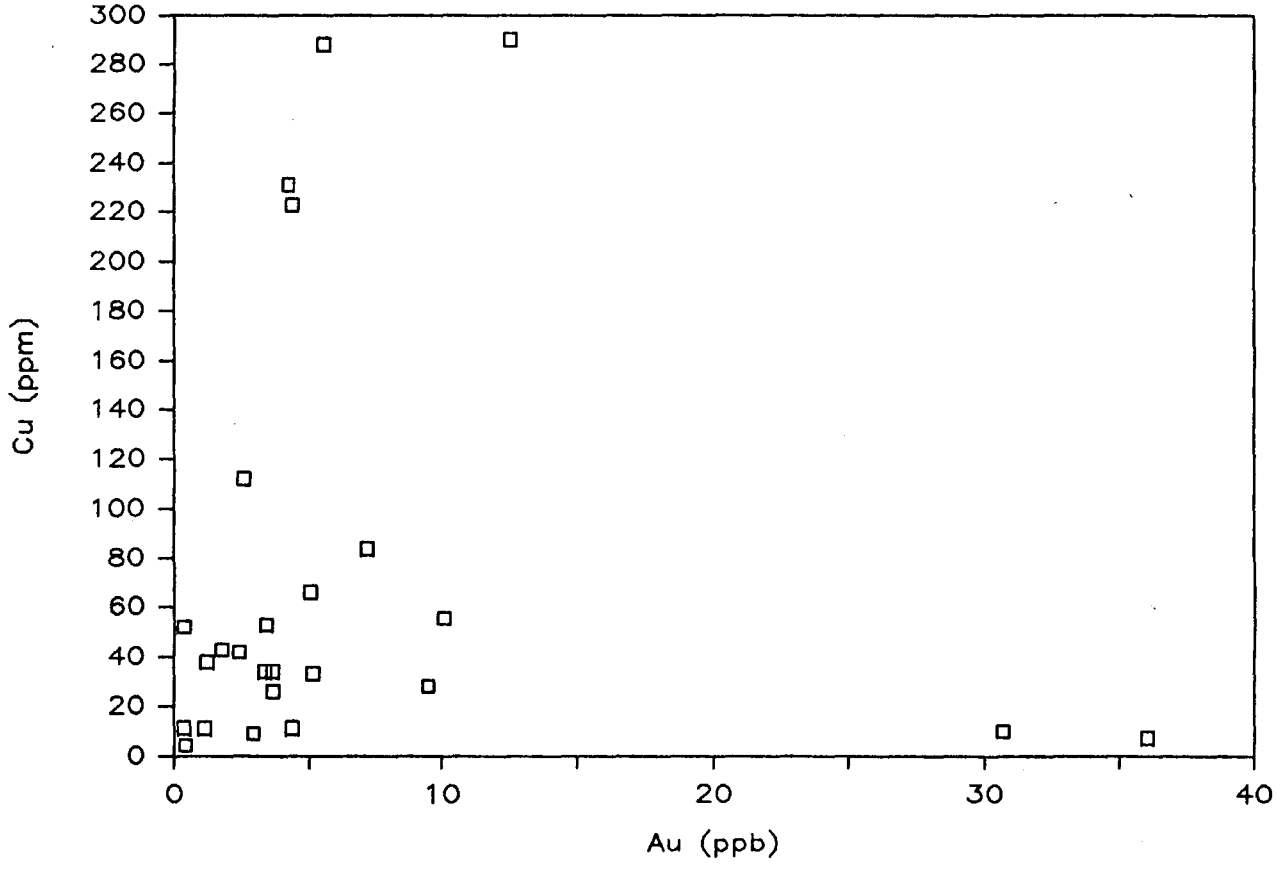

CHAPTER 5

CONCLUSIONS:

The depositional environment of the Boston iron range would have been an ideal site for the deposition of a distal massive sulphide deposit. But, the prevalent base metal in the study area, Zn, occurs in fracture controlled hydrothermal veinlets. Therefore, the base metal mineralization is not related to typical volcanic exhalative massive sulphide deposits. Instead, the mineralization is probably associated with metasomatic processes resulting from contact metamorphism of the Lebel stock on the surrounding rock.

The Au values above background levels (> 10 ppb) are associated with the deformation of the area by the coexistence of high Au values with deformation textures such as cataclastic pyrite and subsequent annealing recrystallization.

Geochemically, Au was found to have a statistically significant positive correlation with W and Zn. If the Au is related to the Zn, then both the Au and Zn may be related to the intrusion of the Lebel stock. But, the highest Au values are not always associated with high Zn contents. The same applies for the converse. The chemical

sediments with > 5 ppm Sb and > 85 ppm As had anomalous Au values but generally were not found to be statistically correlatable.

APPENDIX A

EXPERIMENTAL PROCEDURES

All samples were broken and crushed into pieces up to 1.0 cm in diameter with a chipmunk jaw crusher. These pieces were then crushed with a ceramic lined pulverizer followed by a steel hand pulverizer. The resultant sample powder was then passed through a -200 mesh screen. The sample powder used in the following experimental procedures were all crushed using the above procedure.

LOSS ON IGNITION (LOI) ANALYSIS:

Approximately 1.0 gram of powdered sample was heated at 110°C in a ceramic crucible for approximately 8 hours. This step removed any atmospheric moisture from the sample. The samples were then weighed and reheated at 1000°C for 1.0 hour. This step ignited the volatiles ($CO_2(g)$, $H_2O(g)$, S, F, Cl and to some extent the alkali metals) present in the sample (Maxwell, 1968). The samples were then reweighed. The weight loss for each sample was then calculated and expressed as a percentage of the sample weight recorded after removal of atmospheric moisture.

CO2 DETERMINATION:

Two procedures were used to determine CO2 values of the samples. LECO analysis was used for samples with S contents of less than 4 weight percent while the remaining samples were analyzed using an acid evolution-gravimetric method. Only low S samples were determined by LECO because of SO2 interence on the CO2 analysis.

The acid evolution-gravimetric method, as described by Maxwell (1968), involved the liberation of CO2(g) from 1.0 gram of powdered sample by acid treatment and boiling for 1.5 minutes. The reaction which took place was :

$$CaCO3(s) + 2\ HCl(l) \longrightarrow CaCl2(l) + H2O(g) + CO2(g).$$

The HCl-H2O(g) vapour formed by the process was removed by a condenser attached to the decomposition flask while volatiles liberated by the process were passed through absorbers. The absorbers purified the gas until CO2(g) was the only volatile component left along with the nitrogen carrier gas. A previously weighed CO2-absorption tube was used to remove the purified CO2(g) from the carrier gas. After 0.5 hours, the CO2(g) absorption tube was removed from the system and reweighed. The weight gained by the absorption tube represented the CO2 liberated from the sample and was expressed as a percentage of the original powdered sample weight.

X-RAY FLUORESCENCE ANALYSIS PROCEDURE:

All the geochemical values for S, trace and major elements were obtained by standard x-ray fluorescence (XRF) procedures using powdered pellets and a Phillips 1450 X-Ray Fluorescence Spectrometer. Powder pellets were used instead of fused pellets because many of the samples had sulphur abundances greater than 5 weight percent. This prevented damage to the platinum alloy crucible used to prepare fusion pellets. Powdered pellet analyses is known not to be as accurate as fusion pellets.

POWDER PELLET PREPARATION:

Three to four drops of motor oil was added into approximately 5.0 grams of powdered sample and mixed until uniform. The motor oil acted as an adhesive. The mixture was then put in an aluminum pellet form and compressed to 20 tonnes/square inch.

EPITHERMAL INSTRUMENTAL NEUTRON ACTIVATION ANALYSIS (EINAA) THEORY:

Epithermal instrumental neutron activation analysis (EINAA) was performed to determine Au, As, W and Sb abundances. The following discussion on EINAA is a synthesis of information from Reeves and Brooks (1978) and from a Mac Short Course on NAA (1980) to serve as an outline describing the basic principles of this type of analysis. Neutron activation is based on irradiation of a stable nucleus (such as $^{75}_{33}As$) under a flux of neutrons to produce an isotope with a mass one greater than the original element. An example of a reaction by As due to absorption of thermal neutrons is

$$^{75}_{33}As + ^{1}_{0}n \longrightarrow ^{76}_{33}As + \gamma$$

$$^{76}_{33}As \xrightarrow[26.4\ Hrs.]{\beta^-, \gamma} ^{76}_{34}Se \text{ (stable)}$$

which may also be written as $^{76}_{34}As(n,\gamma)^{76}As$.

If the sample is surrounded by a suitable metal foil, the total neutron flux can be modified. Cadmium is a strong absorber of thermal (low energy) neutrons, but allows good transmission of neutrons with energies above 10 eV (electron volts). Thus, Cd-shielded samples are irradiated by the > 10 eV or epithermal part of the reactor neutron spectrum. Au, As and other elements have high neutron absorption cross sections for epithermal neutrons but, many common major elements such as Na do not.

Therefore, epithermal activation increases the Au/Na ratio of activity compared to full flux thermal neutron activiation.

After cooling, the gamma-rays being emitted are recorded by a Li drifted Germanium semi-conductor detector. The gamma-rays activate conduction band electrons in the detector and generate a flow of current. The gamma ray flux impinging on the detector is directly proportional to the nuclide concentration in the sample. Through the use of built-in computer programs, the spectrometer then separates the significant photopeaks, determines the net photopeak above background energy produced by Compton scattering and calculates the concentration of the element being detected.

EPITHERMAL INSTRUMENTAL NEUTRON ACTIVATION ANALYSIS (EINAA) PROCEDURE:

Approximately 0.5 grams of sample crushed to -200 mesh was weighed and sealed in polyethylene vials. The samples, duplicates and chemical standards, in packages of 15, were irradiated in the McMaster pool type nuclear reactor for 1.0 MWH by a neutron flux of 1.5 x 10EE13 neutrons/cm. sq./sec. The samples were rotated during the irradiation and shielded with cadmium. They were then allowed to cool for approximately 59 hours after irradiation. Normal counting procedures were then performed for As and Sb using a coaxial intrinsic Germanium detector capabled to a Canberra Series 80 multichannel analyzer (MCA) . The detector has an 18.4 cm active area, 55 cm active volume and a 0.05 cm window thickness. The energy resolution is less than 0.85 keV at 122 keV and 1.8 keV at 1.332 MeV with a relative efficiency of greater than 10% and a peak to Compton ratio of 35:1. Data from the MCA was read out on punched paper tape. Approximately 110 hours after irradiation, counting was resumed for Au and W using the same irradiated samples and apparatus as before. The activity recorded by the spectrometer was then used to calculate the orignal activity at the start of the cooling period using the decay equation:

$$A_t = A_o e^{-\lambda t}$$

where A_t = activity at time t (spectrometer reading)

A_o = original activity (at time zero)

t = time elapsed since the start of the cooling period.

λ = decay constant for a particular element

$$\lambda = \frac{0.693147}{\text{elemental half-life } (T_{\frac{1}{2}})}$$

The calculated original activity (corrected count rate) was then divided by the average number obtained from the standards for a particular element and was then converted into ppm by dividing the value with the weight of the sample. A ppb value was obtained by dividing the ppm value by 1000. The experimental and calculation procedure has been previously tested to have a sensitivity level of 5 ppb for Au and 0.01 ppm for As, Sb and W.

APPENDIX B

ERROR ANALYSIS:

TABLE 1: GEOCHEMICAL DATA ERRORS

ELEMENT	ERROR(%)	ELEMENT	ERROR(%)	VOLATILES	ERROR(%)
Au	20.55	SiO2	.83	LOI	3.37
As	20.9	Al2O3	2.93	S	10.95
W	83.06	Fe2O3	5.97	CO2	2.83
Sb	32.7	MgO	5.16		
Cu	8.27	CaO	3.1		
Pb	12.8	Na2O	4.26		
Zn	20.45	K2O	5.7		
Ni	27.35	TiO2	0		
Co	19.1	MnO2	0		
Cr	40.44	P2O5	0		
V	12.7				

Error values in Table 1 were calculated using the pooled variance estimate of precision error using the equation from Dixon and Massey (pg. 145, 1957):

$$Sp^2 = \frac{\sum_{j=1} \sum_{i=1} (X_{ij} - \bar{X}_j)^2}{\sum_j n_j - k}$$

where X_{ij} = value of the ith replicate of the jth sample.

$\bar{X}$ = mean value for the jth sample.

k = total number of samples (6).

n_j = number of replicates in the jth sample (3).

This value was then converted into a coefficient of variance expressed as a percentage:

$$C = \frac{100 \cdot Sp}{\bar{X}}$$

where $\bar{X}$ = grand mean for all samples.

LINEAR REGRESSION:

The plots derived by linear regression were tested at the 95% significance level using a t-test. A sample calculation would proceed as followed:

For Co vs. Ni:

From linear regression the variance = $r^2 = 0.47$

therefore, the correlation coefficient = $\sqrt{r^2} = 0.6856$

$$t = \frac{r\sqrt{N-2}}{\sqrt{1-r}}$$

where r= correlation coefficient.
N= total number of points in sample set under consideration.

$$= \frac{(0.6856)(24-2)^{\frac{1}{2}}}{[\,1-(0.6856)^2\,]^{\frac{1}{2}}}$$

$$= 4.474 > 1.717$$

(from Davis, pg. 95, 1973)

Since t > 1.717, then there is a correlation at the 95% significance level between Co and Ni.

REFERENCES

Blum, N. 1985. Ph.D. Thesis, McMaster University, in prep.

Cameron, E.M. and Garrels, R.M. 1980. Geochemical compositions of some Precambrian shales from the Canadian Shield. Chemical Geology, v. 28, pp. 181-197.

Coad, P.R. 1979. Nickel sulphide deposits associated with ultramafic rocks of the Abitibi belt and economic potential of mafic-ultramafic intrusions. Ontario Geological Survey Study 20, 84p.

Colvine, A.C., Andrews, A.J., Cherry, M.E., Durocher, M.E., Fyon, J.A., Lavigne, Jr., M.J., Macdonald, A.J., Marmont, S., Poulsen, K.H., Springer, J.S. and Troop, D.G. 1984. An integrated model for the origin of Archean lode gold deposits, Ontario Geological Survey, Open File Report 5524, 98p., 7 tables, 53 figs., and 2 appendices.

Crocket, J.H., McNutt, R.H., Schwarcz, H.P., Rees, C.E., Blum, N., Hurley, T., Bowins, R. and Kabir, A. 1983. Isotopic and geochemical characterization of Archean iron formations and associated volcanic rocks - some preliminary results from the Temagami and Boston Iron Formations; Grant 132, pp. 29-40 in Geoscience Research Grant Program, Summary of Research 1982-83, edited by E.G. Pye, Ontario Geological Survey, Miscellaneous Paper 113, 199p.

Davis, J.C. 1973. Statistics and Data Analysis in Geology. John Wiley and Sons, Inc., Toronto. 550p.

Deer, W.A., Howie, R.A. and Zussman, J. 1980. An Introduction to the Rock Forming Minerals. Clowes and Sons, Ltd., London. 528p.

Dixon, W.S. and Massey, F.J. 1957. Introduction to Statistical Analysis, 2nd ed. McGraw-Hill, Inc., Toronto. 145p.

Dubuc, F. 1972. Geology of the Adams Mine. Unpublished manuscript. 12p.

Goodwin, A.M. 1977. Archean volanism in Superior Province, Canadian Shield; pp. 205-242 in Volcanic Regimes in Canada, edited by W.R. Baragar, L.C. Coleman, and J.M. Hall, Geological Association of Canada, Special Paper Number 16, 476p.

Gross, G.A. 1965. Geology of iron deposits in Canada. I: general geology and evaluation of iron deposits. Geological Survey of Canada Economic Geology Report 22, v. 1, 181.p.

Groves, D.I., Barrett, F.M. and McQueen, K.G. 1980. Geochemistry and origin of cherty metasediments within ultramafic flow sequences and their relationship to nickel mineralization; pp. 57-69 in Archean Cherty Metasediments: Their Sedimentology, Micropaleontology, Biochemistry, and Significance to Mineralogy, edited by J.E. Glover and D.I. Groves, p. 88.

Hausen, D.M. 1981. Process mineralogy of the auriferous pyrite ores at Carlin, Nevada; pp. 271-289 in Process Mineralogy, Extractive Metallurgy, Mineral Exploration, Energy Resources, edited by D.M. Hausen and W.C. Park, Conference Proceedings, The Metallurgical Society of American Institute of Mining, Metallurgical and Petroleum Engineers.

Hewitt, D.F. 1949. Geology of Skead Township, Larder Lake Area. Ontario Department of Mines, v. 58, pt. 6, 43p.

Jensen, L.S. 1976. Regional stratigraphy and structure of the Timmins-Kirkland Lake Area, District of Cochrane and Timiskaming and Kirkland Lake-Larder Lake Areas, District of Timiskaming; pp. 87-95 in Summary of Field Work, 1976, by the Geological Branch, edited by V.G. Milne, W.R. Cowan, K.D. Card, and J.A. Robertson, Division of Mines Miscellaneous Paper 67, 183p.

---------- 1977. Regional stratigraphy and structure of the Timmins-Kirkland Lake Area District of Cochrane and Timiskaming and Kirkland Lake-Larder Lake Areas, District of Timiskaming; pp. 98-101 in Summary of Field Work, 1977, by the Ontario Geological Survey, edited by V.G. Milne, O.L. White, R.B. Barlow and J.A. Robertson, Ontario Geological Survey Miscellaneous Paper 75, 208p.

---------- 1978(a). Archean komatiitic, tholeiitic, calc-alkalic and alkalic volcanic sequences in the Kirkland Lake Area, in Toronto '78 Field Trips Guidebook, edited by A.L. Currie and W.O. Mackasey, Geological Association of Canada, 361p.

---------- 1978(b). Regional stratigraphy and structure of the Timmins-Kirkland Lake Area, District of Cochrane and Timiskaming and the Kirkland Lake-Larder Lake Area, District of Timiskaming; pp. 67-72 in Summary of Field Work, 1978, by the Ontario Geological Survey, edited by

V.G. Milne, O.L. White, R.B. Barlow and J.A. Robertson, Ontario Geological Survey Miscellaneous Paper 82, 235p.

Jensen, L.S. 1979. Larder Lake synoptic mapping project; pp. 64-69 in Summary of Field Work, 1979, by the Ontario Geological Survey, edited by V.G. Milne, O.L. White, R.B. Barlow, and C.R. Kustra, Ontario Geological Survey Miscellaneous Paper 90, 245p.

Jolly, W. 1974. Metamorphism in the Canadian Shield. Geological Survey of Canada, Paper 78-10, pp. 63-79.

Lawton, K.D. 1957. Geology of Boston Township and part of Pacaud Township. Ontario Department of Mines, Sixty-sixth Annual Report, 55p. Accompanied by Map No. 1957-4, Scale 1 inch to 1000 feet. Volume LXVI, Part 5.

Maxwell, J.A. 1968. Rock and Mineral Analysis. Interscience Publishers, New York. 584p.

McRoberts, G. 1985. M.Sc. Thesis, McMaster University, in prep.

Mineralogical Association of Canada 1980. Short Course in Neutron Activation Analysis in the Geosciences, edited by G.K. Muecke, 279p.

Moorehouse, W.W. 1959. The Study of Rocks in Thin Section. Harper and Row, Inc., New York, N.Y., 514p.

Muir, J.E. and Comba, C.D.A. 1979. The Dundonald deposit: an example of volcanic-type nickel sulphide mineralization. Canadian Mineralogist, v. 17, pp. 351-359.

Reeves, R.D. and Brooks, R.R. 1978. Trace Element Analysis of Geological Materials. John Wiley and Sons, Inc., New York, N.Y., 421p.

Ridler, R.H. 1970. Relationship of mineralization to volcanic stratigraphy in the Kirkland-Larder Lakes Area, Ontario. Geological Association of Canada, Proceedings, v. 21, pp. 33-42.

Spry, A. 1976. Metamorphic Textures. Permagon Press Ltd., Toronto. 350p.

Stanton, R.L. 1972. Ore Petrology. McGraw-Hill, Inc., New York, 713p.

Taylor, S.R. 1964. The abundance of chemical elements in

the continental crust - a new table. Geochimica Cosmochimica Acta, v. 28, pp. 1273-1285.

Turner, Francis J. 1981. Metamorphic Petrology: Mineralogical, Field, and Tectonic Aspects. 2nd edition Hemisphere Publishing Corporation, New York, N.Y. 524p.

Viljoen, M.J. and Viljoen, R.P. 1969. The geology and geochemistry of the lower ultramafic unit of the Onverwacht Group and a proposed new class of igneous rock. Special Publication of the Geological Society of South Africa, v. 2, pp. 221-244.

Walker, R.G. 1978. A critical appraisal of Archean basin-craton complexes. Canadia Journal of Earth Sciences, v. 15, pp. 1213-1218.

Wells, J.D. and Mullens, T.E. 1973. Gold-bearing arsenian pyrite determined by microprobe analysis, Cortez and Carlin Gold Mines, Nevada. Economic Geology, v. 68, pp. 187-201.

Wilson, G.C. 1985. The role of free carbon in metallic mineral deposits, University of Toronto Isotrace Laboratory Report 1985-1. 58p.

SAMPLE LOCATION AND GEOLOGY OF THESIS AREA

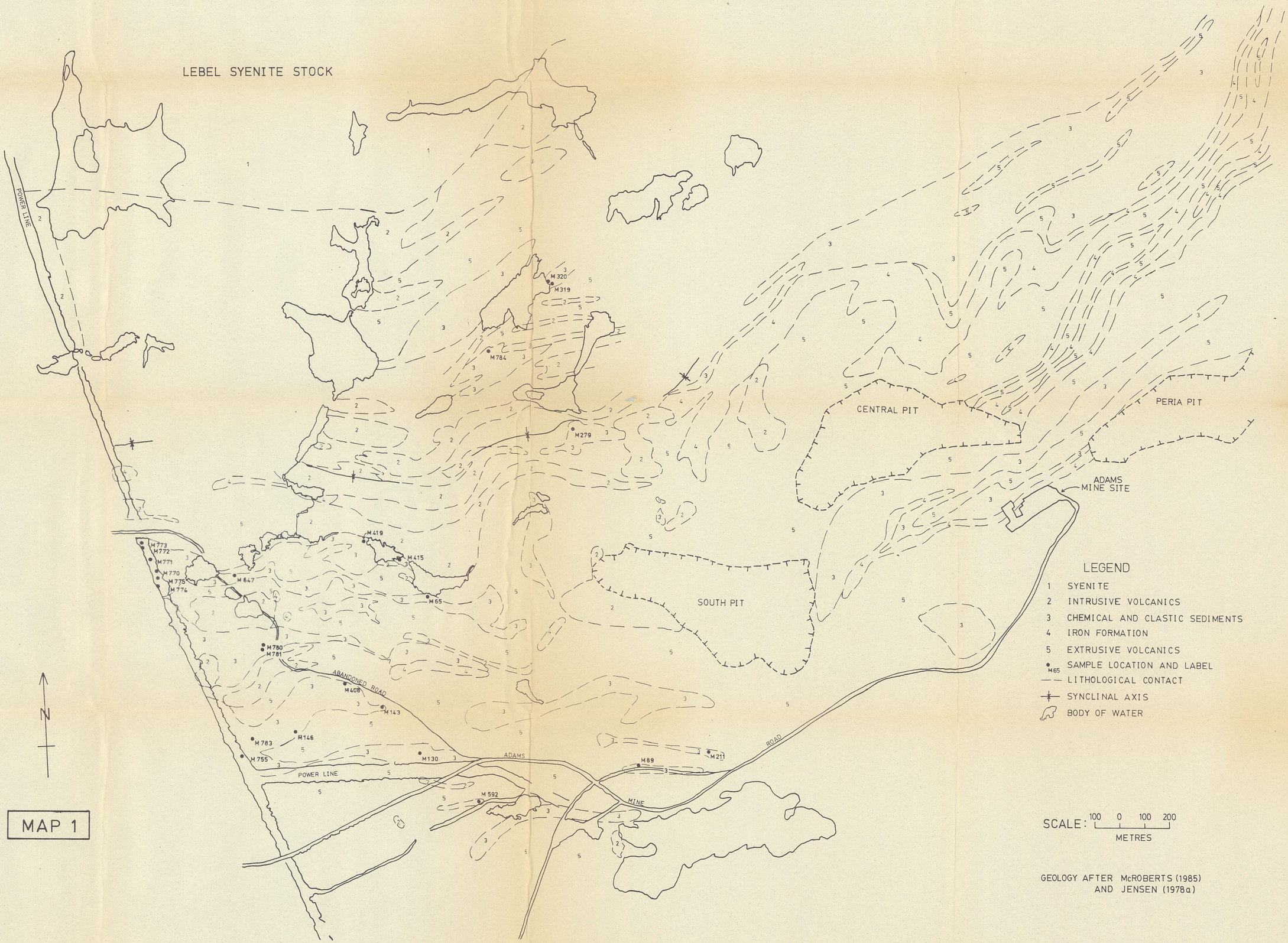

GEOLOGY AFTER McROBERTS (1985)
AND JENSEN (1978a)